CERN-TH/97-210

MSSM Higgs searches in multi-b-jet final states at the LHC

Elżbieta Richter-Wąs[1]
CERN, TH Division, 1211 Geneva 23, Switzerland
Institute of Computer Science, Jagellonian University,
Institute of Nuclear Physics
30-059 Kraków, ul.Kawiory 26a, Poland

Daniel Froidevaux
CERN, PPE Division, 1211 Geneva 23, Switzerland

Abstract

This paper discusses the possibility to observe a signal from MSSM Higgs boson decays into final states containing four b-jets. Two specific channels are considered: $b\bar{b}H$ and $b\bar{b}A$ production with $H, A \to b\bar{b}$, for large values of m_H, m_A and $\tan\beta$, and $H \to hh \to b\bar{b}b\bar{b}$ decays for 150 GeV $< m_H < 2m_t$ and for low values of $\tan\beta$. Both channels are difficult to extract because of the very large reducible and irreducible QCD backgrounds. Even with an ultimate integrated luminosity, expected per LHC experiment, of $3 \cdot 10^5$ pb^{-1}, the region of the MSSM parameter space covered by these channels does not extend the reach beyond that accessible to other channels that were studied in the past. Nevertheless, their observation would help in constraining the couplings and branching ratios of the MSSM Higgs bosons.

CERN-TH/97-210
August 1997

[1] Supported in part by Polish Government grants 2P03B00212 and 2P03B17210.

1 Introduction

One of the most attractive theoretical extensions of the Standard Model (SM) is the Minimal Supersymmetric Standard Model (MSSM)[1, 2]. Recently, the interest in this model has grown for several reasons. It is the simplest version of low-energy supersymmetry, with the minimal gauge group and particle content compatible with phenomenology. It preserves all SM predictions at low energies, and is therefore not contradicted by any of the precision measurements at LEP [3]. It also has a high level of predictivity in the Higgs sector. At tree level, all Higgs-boson masses and couplings can be expressed in terms of only two parameters, usually chosen to be the ratio of the vacuum expectation values of the two Higgs doublets, $\tan\beta$, and the mass of the A boson, m_A. Radiative corrections [4] introduce a dependence of the masses and couplings on the top-quark mass, the squark masses and the mixing parameters in the stop–sbottom sector. All couplings of the MSSM Higgs bosons to fermions and bosons can be obtained from the SM couplings by multiplying the latter with the appropriate MSSM correction factors, which depend on the parameters listed above.

The MSSM predictions concerning the Higgs-boson masses have important phenomenological consequences. One of the Higgs bosons, the scalar h, is relatively light, with a maximum allowed mass value varying from 105 to 153 GeV, depending on the MSSM parameters and the top-quark mass. The masses of the other Higgs bosons are expected to be larger and nearly degenerate for $m_A > 200$ GeV.

There are a variety of production and decay channels through which the MSSM Higgs bosons can be observed at LHC [5]. Some of these are similar to the SM, such as the H, $h \rightarrow \gamma\gamma$ or $H \rightarrow 4\ell$ channels. Others are allowed in the SM but have large enough rates only in the MSSM case, e.g. $H, A \rightarrow \tau\tau,\ \mu\mu$, and $t\bar{t}$. There are also channels characteristic of the MSSM, such as $H^{\pm} \rightarrow \tau\nu$, $A \rightarrow Zh$, $H \rightarrow hh$, as well as the production of h bosons in squark and gluino decays.

The work described in [5] presents an extended and complete study of most of these channels, leading to realistic predictions for the LHC discovery potential in the MSSM Higgs sector. Figures 1 and 2 show the final results of [5], namely the 5σ-discovery contour curves, for $m_t = 175$ GeV and for integrated luminosities of $3 \cdot 10^4$ pb^{-1} and $3 \cdot 10^5$ pb^{-1} per LHC experiment, respectively, which represent the integrated luminosities expected after three and ten years of operation. With the initial, modest integrated luminosity of $3 \cdot 10^4$ pb^{-1}, a large fraction of the parameter space is already covered. With the ultimate integrated luminosity of $3 \cdot 10^5$ pb^{-1}, the LHC discovery potential maps the complete parameter space. For the vast majority of cases, the experiment would be able to distinguish between the SM and MSSM cases.

The MSSM Higgs sector is quite challenging experimentally for the LHC [6], since, most often, the signal-to-background ratios are much smaller than unity and the detector resolution in several of the accessible channels is far from optimal. This sets stringent requirements on the performance in terms of energy and momentum

resolution and of particle identification; however, on the other hand, the variety of channels makes this sector an excellent benchmark to evaluate the discovery potential of the detector. A very good performance of the electromagnetic calorimeter, excellent b-tagging capabilities, good E_T^{miss}-resolution and τ-identification are all crucial ingredients to fully explore the MSSM Higgs sector.

Channels with b-jets identified in the final state were considered so far only if associated with hard leptons or photons: Wh with $h \to b\bar{b}$, $H/A \to t\bar{t} \to \ell\nu jjb\bar{b}$, $A \to Zh \to \ell\ell b\bar{b}$ and $H \to hh \to b\bar{b}\gamma\gamma$. All of these channels were found to be observable only for low values of $\tan\beta$. The possibility to improve the sensitivity by using identified b-jet spectators was also recently considered [7] in the case of $b\bar{b}A, b\bar{b}H$ production with $H/A \to \tau\tau$ decay. In all these cases, however, isolated leptons or photons provide a straightforward experimental trigger, and the purely hadronic background from QCD multi-jet production is not a source for concern.

Final states containing more than two b-jets have not been explored so far in these searches. They nevertheless deserve some attention, since they correspond to the dominant production and decay modes of the MSSM Higgs bosons over a large fraction of the parameter space. Also, it has been reported in recent theoretical papers [8] that they should be very promising for discovery in the MSSM Higgs sector.

Two possible channels will be discussed in this paper[2], both leading to final states containing four b-jets but no lepton nor photon for the experimental trigger.

- The first channel arises from $b\bar{b}H$ and $b\bar{b}A$ production, which is strongly enhanced for large values of $\tan\beta$, since the production rates grow like $\tan^2\beta$. These production processes were studied so far through the $\tau\tau$ and $\mu\mu$ decay modes over the mass range from 100 to 500 GeV. The $\tau\tau$ channel requires excellent τ-identification to suppress the huge background of hadronic jets from various sources, but also excellent E_T^{miss}-resolution for the reconstruction of the $\tau\tau$ invariant mass. The region of parameter space accessible to the $\tau\tau$ channel, which has a branching ratio of $\sim 10\%$, is superior to that of the $\mu\mu$ channel; for $m_A = 300$ GeV, the 5σ-discovery contour extends down to $\tan\beta \sim 10$ for an integrated luminosity of $3 \cdot 10^4$ pb^{-1}, and down to $\tan\beta \sim 7$ for ATLAS+CMS combined with an integrated luminosity of $3 \cdot 10^5$ pb^{-1} per experiment. For larger masses, the sensitivity degrades rapidly, due to the decreasing production rates and the degradation of the $\tau\tau$ mass resolution. For $m_A = 500$ GeV, the accessible region reaches only down to $\tan\beta \sim 25$ (resp. ~ 18) for an integrated luminosity of $3 \cdot 10^4$ pb^{-1} (resp. $3 \cdot 10^5$ pb^{-1}). The rates expected for the $b\bar{b}$ decay mode would be much higher, since the branching ratio is about 90%. However, the observation of final states containing multiple b-jets is very challenging: it requires excellent b-tagging performance and very efficient jet reconstruction.

[2] The present paper is a slightly modified version of [9].

- The second channel is the $H \to hh$ decay, which is dominant for low values of $\tan\beta$ and for $m_H < 2m_t$. The observation of this channel would be very interesting, since it would correspond to the simultaneous discovery of two MSSM Higgs bosons. The final state $H \to hh \to bb\gamma\gamma$ has been studied so far. It provides a straightforward experimental trigger and offers good kinematical constraints and mass resolution for the reconstruction of m_H. The expected rates are, however, very low, even when requiring only one identified b-jet in the final state. The sensitivity to this channel decreases as $\tan\beta$ increases, and the accessible region of parameter space extends up to $\tan\beta \sim 2.5$ for an integrated luminosity of $3 \cdot 10^4$ pb^{-1} and up to $\tan\beta \sim 4.5$ for ATLAS+CMS combined with an integrated luminosity of $3 \cdot 10^5$ pb^{-1} per experiment. The $H \to hh \to b\bar{b}b\bar{b}$ channel would yield much higher rates, by a factor of almost 1000; however, the 4-jet final state will be difficult to trigger on and to extract from the huge QCD background.

The main difficulty and uncertainties in the analysis presented here arise from the evaluation of the QCD multi-jet/multi-b-jet backgrounds. There are many sources of uncertainties in the predictions for QCD multi-jet production: the parton density functions, the choice of scale for the strong coupling constant, the calculations of the exact and complete matrix elements and the higher-order corrections. At tree level, matrix elements for all parton processes with at most five partons in the final state, have been calculated and embedded in a Monte Carlo generator called NJETS [10]. However, the parton-flavour information is not accessible in this generator. For the studies presented here, the PYTHIA Monte Carlo generator [11], with its QCD parton-shower modelling and gluon splitting into heavy quarks, has been used, since the flavour content of the jets in the final state is of crucial importance for the evaluation of many of the background processes. Only leading-order terms are controlled in this approach. Predictions from both generators for events with at least 2, 3, 4 reconstructed high p_T jets ($p_T^{jet} > 30$, 40, 50 GeV) were compared and results from PYTHIA were found to be systematically lower by a factor 2-3. The uncertainties on the predictions for high-p_T multi-jet final states are therefore estimated to be as high as at least a factor of 3 and the results presented throughout this paper as background rates should be considered as an optimistic.

The expected detector performance is simulated with the ATLFAST package [12]. This package, used extensively for fast simulation of the ATLAS detector response provides reliable estimates of the detector response to hadronic jets. Though the parameterisations of the detector performance are ATLAS–specific, the results presented here can be considered as representative of what is to be expected at the LHC. For those results evaluated in the case of high-luminosity operation, pile-up effects are included. The reconstructed jet energies, after kinematical selection, are recalibrated, as explained in [12], to obtain the correct peak position for e.g. the $m_{b\bar{b}}$ distribution. For the analysis presented here, a rather optimistic b-tagging performance is assumed (see [13] for the most recent ATLAS results); for the low-luminosity case, an overall b-tagging efficiency of $\epsilon_b = 60\%$ is assumed, with a rejec-

tion against c-jets of $R_c = 10$ and against light-quark and gluon jets of $R_j = 100$. For the high-luminosity case, the b-tagging efficiency is degraded to $\epsilon_b = 50\%$, assuming the same rejection against non-b-jets.

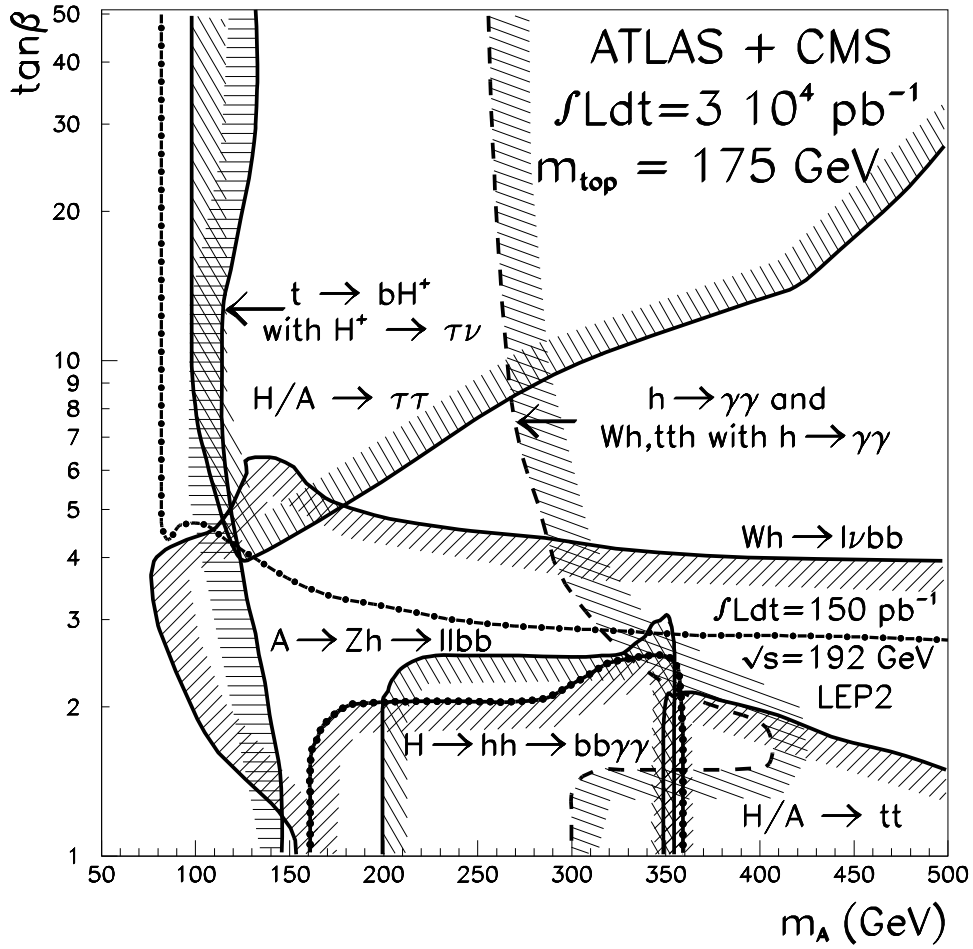

Figure 1: *For* $m_t = 175$ *GeV and an integrated luminosity of* $3 \cdot 10^4$ pb^{-1}*, expected LHC (ATLAS + CMS)* 5σ*-discovery contour curves in the* $(m_A, \tan\beta)$ *plane for all MSSM Higgs-boson channels studied in [5].*

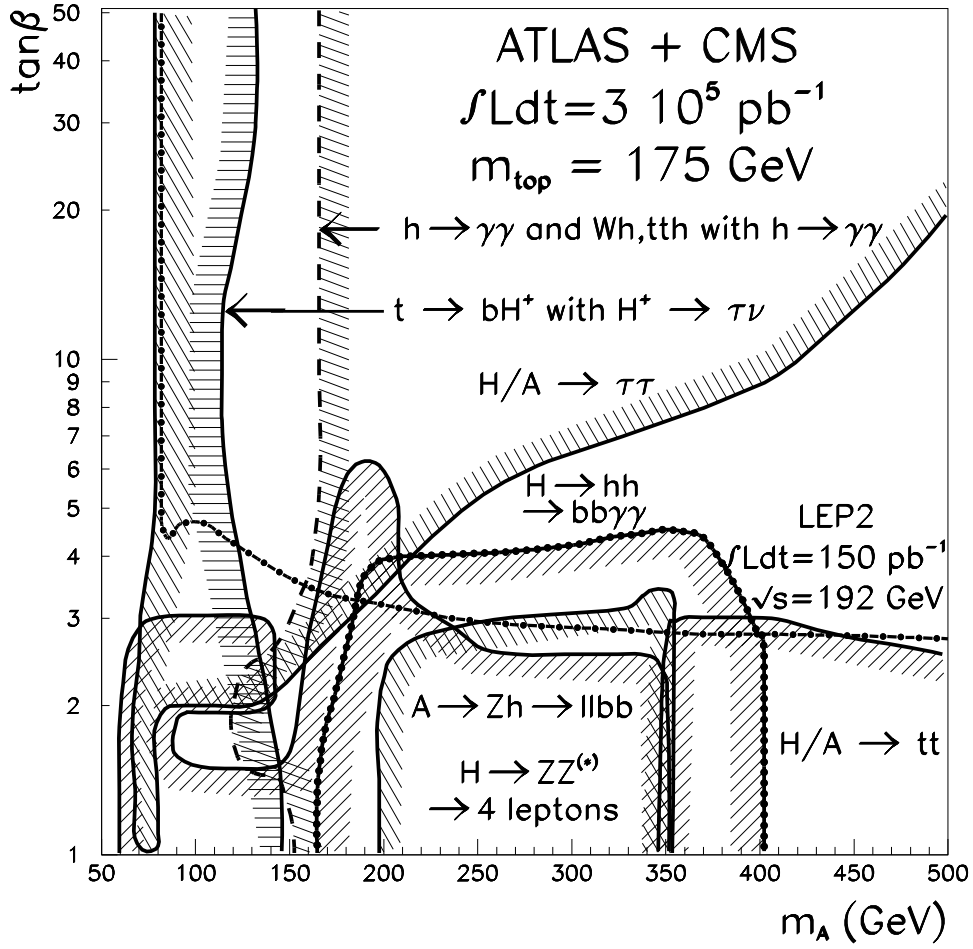

Figure 2: *For* $\mathrm{m_t}$ *= 175 GeV and an integrated luminosity of* $3 \cdot 10^5$ pb^{-1}*, expected LHC (ATLAS + CMS)* 5σ*-discovery contour curves in the* ($\mathrm{m_A}$, $\tan\beta$) *plane for all MSSM Higgs-boson channels studied in [5].*

Two questions are of particular interest in the context of these studies:

• Is it possible, using the $b\bar{b}H/A$ channel with $H/A \to b\bar{b}$, to extend the region in parameter space already covered by the $\tau\tau$ channel, particularly to values of m_A larger than 500 GeV?

• Is it possible, using the $H \to hh \to b\bar{b}b\bar{b}$ channel, to extend the region in parameter space already covered by the $H \to hh \to b\bar{b}\gamma\gamma$ channel?

2 Observability of $H/A \to b\bar{b}$ for large $\tan\beta$

2.1 Signal events

For large values of m_H and m_A, the final state in this channel has a very characteristic topology: the two hardest jets in the event come from the $H/A \to b\bar{b}$ decay, while the softer ones come from the associated $b\bar{b}$ production and from initial/final-state radiation. These features have been used for the event selection. At least four reconstructed jets are required in the final state, with the three or four jets of highest transverse energy tagged as b-jets. The two jets with the largest transverse energy are used for the reconstruction of the Higgs-boson mass, $m_{b\bar{b}}$. The selection criteria have been optimised for each value of m_A and m_H, chosen from 300 to 900 GeV, as follows:

- at least four reconstructed jets (ordered in decreasing p_T) with $p_T^{j3} > 50$ GeV and $p_T^{j4} > 30$ GeV; the thresholds on the two hardest jets are raised to:
  - $p_T^{j1} > 100$ GeV and $p_T^{j2} > 70$ GeV (selection S_{300});
  - $p_T^{j1} > 200$ GeV and $p_T^{j2} > 100$ GeV (selection S_{500});
  - $p_T^{j1} > 250$ GeV and $p_T^{j2} > 150$ GeV (selection S_{700});
  - $p_T^{j1} > 300$ GeV and $p_T^{j2} > 200$ GeV (selection S_{900});
- the three highest-p_T jets are required to be tagged as b-jets; an additional tagged b-jet is required in two different approaches:
  - in algorithm A, the fourth highest-p_T jet is chosen;
  - in algorithm B, any tagged b-jet among the additional jets is accepted;
- the two highest-p_T jets are used to reconstruct the $m_{b\bar{b}}$ distribution;
- the events are accepted if $m_{b\bar{b}}$ falls within ± 80 to 100 GeV of the considered Higgs-boson mass; the mass window was chosen to accept approximately 70% of the signal events.

The acceptance of the selection S_{500} increases from 10% to 40% as the Higgs-boson mass increases from 500 to 900 GeV, as shown in Table 1. The three highest-p_T jets are found to be true b-jets only in 6% to 14% of the events, due to initial/final-state radiation. This proportion decreases to 1.6% to 3.2% of the events if the fourth highest-p_T jet is also required to be a true b-jet (algorithm A). For algorithm B, the acceptance is improved by about 60%. These rather low acceptances for the signal events are unavoidable to reduce the huge QCD backgrounds to an acceptable level, as discussed in Section 2.2. It was checked for example that the fact of requiring any combination of the reconstructed jets to be identified as b-jets leads to much worse signal-to-background ratios and significances.

Table 2 shows, for an integrated luminosity of $3 \cdot 10^5$ pb^{-1}, the expected rates of signal events after applying the selection S_{500} and the b-tagging procedure, for different assumptions on the b-tagging performance in addition to the default one described above. The signal sample is dominated by events containing true b-jets: the contribution from events with at least one mis-identified jet is below 10%, as shown by comparing the results for the default jet rejections with those for an almost infinite rejection, R = 10^6.

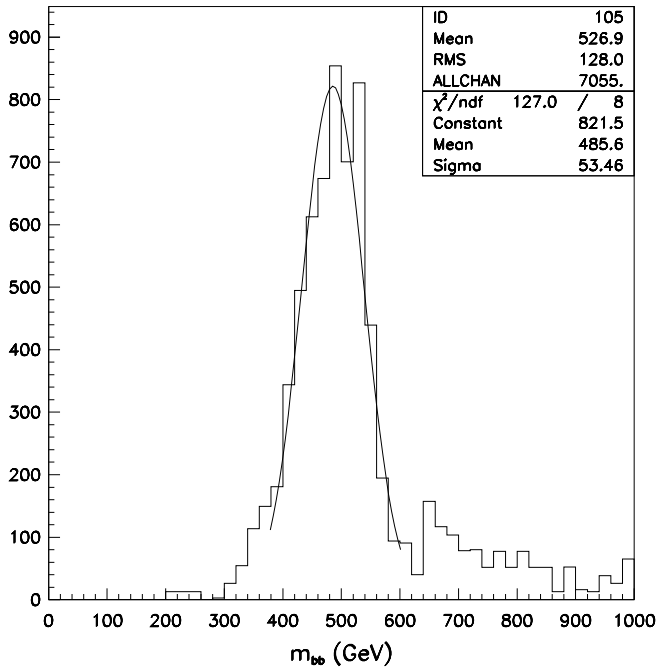

Figure 3: *Reconstructed* $m_{b\bar{b}}$ *mass after applying the selection* S_{500}*, for the* $b\bar{b}H$ *signal with* $H \rightarrow b\bar{b}$ *decay and for* m_H *= 500 GeV. The degradation in resolution expected from pile-up at high luminosity has been included.*

Table 1: *Acceptance of selection S_{500} and fractions of events containing one or more true b-jets, for three values of* m_A *and* m_H.

bbH, bbA with $H/A \to b\bar{b}$ Selection S_{500}	σ (pb)	Four jets	Jet1 = true b-jet	+ jet2 = true b-jet	+ jet3 = true b-jet	Algorithm A	Algorithm B
m_H = 500 GeV	3.5	10.8%	10.0%	8.4%	5.6%	1.6%	2.4 %
m_H = 700 GeV	0.9	20.4%	18.0%	14.8%	8.0%	2.0%	3.2 %
m_H = 900 GeV	0.2	39.2%	36.0%	26.4%	13.6%	3.2%	5.5 %

Table 2: *Expected rates of reconstructed signal events after applying selection* S_{500} *and b-tagging, for* $\tan\beta = 30$ *and for an integrated luminosity of* $3 \cdot 10^5$ pb^{-1} *(ATLAS). The results are shown for three different assumptions on the b-tagging performance.*

Selection S_{500} m_A, m_H	Four jets	Jet1 tagged as b-jet	+ jet2 tagged as b-jet	+ jet3 tagged as b-jet	Algorithm A	Algorithm B
	$\epsilon_b = 0.5$, $\epsilon_c = 10^{-6}$, R = 10^6					
500 GeV	111000	52400	22000	7250	1090	1670
700 GeV	54600	24700	9850	2660	363	572
900 GeV	23800	10700	4030	1030	125	217
	$\epsilon_b = 0.5$, $\epsilon_c = 0.1$, R = 10^2					
500 GeV	111000	52500	22100	7400	1180	1770
700 GeV	54600	24700	9940	2750	404	622
900 GeV	23800	10700	4080	1070	142	238
	$\epsilon_b = 0.6$, $\epsilon_c = 0.1$, R = 10^2					
500 GeV	111000	63000	31900	12700	2420	3630
700 GeV	54600	29700	14300	4730	824	1270
900 GeV	23800	12900	5860	1830	288	486

The reconstructed $m_{b\bar{b}}$ peak is rather broad, because final-state radiation and hadronisation degrade the mass resolution and also because a significant fraction (about 20%) of the $b\bar{b}$ combinations entering the distribution are incorrect (one or both b-jets do not originate from the $H \to b\bar{b}$ decay). Figure 3 shows as an example the distribution of the reconstructed $m_{b\bar{b}}$ for m_H = 500 GeV; the acceptance in the chosen mass bin ($m_H \pm 80$ GeV) is about 70%.

The quality of the mass reconstruction has been studied separately, using the $gg \to H \to b\bar{b}$ process, which does not suffer from the combinatorial backgrounds

of the $b\bar{b}H$ process. The mass resolution obtained and the acceptance in the mass window are shown in Table 3 and in Fig. 4 for all events without any selection. The large tails in the mass distributions that can be seen in Fig. 4 are almost completely removed if one applies the selection criteria on the jet transverse energies, but the events in the tails are nevertheless lost. Most of these losses are accounted for in the acceptances quoted in Table 1. Finally, Table 4 shows the total expected signal rates for three values of m_H and the appropriate selection cuts, before and after applying the chosen $m_{b\bar{b}}$ mass window (including pile-up at high luminosity), for an integrated luminosity of $3 \cdot 10^5$ pb^{-1}.

Table 3: *Mass resolutions expected for the reconstructed* $m_{b\bar{b}}$ *mass, for the* $gg \to H \to b\bar{b}$ *process in the absence and presence of pile-up. No selection cuts are applied.*

Higgs mass (GeV)	No pile-up		With pile-up	
	σ_m (GeV)	Within $\pm$ 2 σ_m	σ_m (GeV)	Within $\pm$ 2 σ_m
300	22.7	62%	26.4	60%
500	33.8	57%	39.7	55%
700	38.3	52%	44.0	50%
900	52.6	53%	63.5	52%

Table 4: *Expected numbers of signal events after applying the appropriate selection criteria, for an integrated luminosity of* $3 \cdot 10^5$ *pb*$^{-1}$ *(ATLAS). The numbers of events accepted within the* $m_{b\bar{b}}$ *mass window are shown in brackets.*

bbH, bbA production with $H/A \to b\bar{b}$	Kinematical cuts	Three b-jets	Algorithm A	Algorithm B
$m_H = 500$ GeV Selection S_{500}	$1.1 \cdot 10^5$	7400 (5000)	1100 (960)	1800 (1300)
$m_H = 700$ GeV Selection S_{700}	$3.4 \cdot 10^4$	2289 (1530)	360 (240)	530 (350)
$m_H = 900$ GeV Selection S_{900}	$1.3 \cdot 10^4$	900 (524)	135 (80)	210 (122)

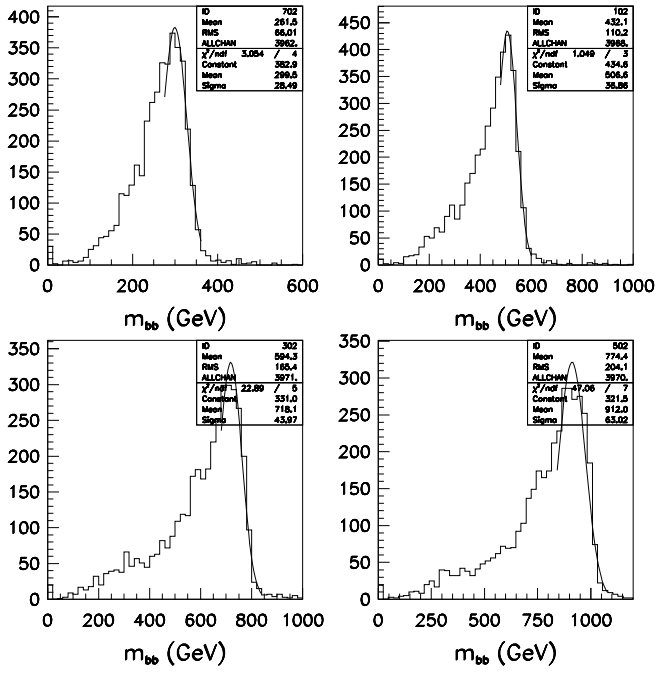

Figure 4: *Reconstructed* $m_{b\bar{b}}$ *before any selection cuts, for the* $gg \rightarrow H \rightarrow b\bar{b}$ *process and for* m_H *= 300, 500, 700 and 900 GeV. The degradation in resolution expected from pile-up at high luminosity has been included.*

2.2 Background events

The background to the $b\bar{b}H/A$ signal with $H/A \rightarrow b\bar{b}$ decay is completely dominated by QCD multi-jet processes with final states containing a variable number of real b-jets. For the analysis presented here, large samples of background events were generated using PYTHIA, based on the hard-scattering di-jet sub-processes. The hard-scattering process was accompanied by initial-state radiation, which provides one of the sources of additional jets; gluon splitting and/or final-state radiation also provide a source of additional jets, some of which originate from b-quarks.

The event generation was organised in several p_T bins with different statistics, typically $5 \cdot 10^4$ events to $4 \cdot 10^6$ events per bin. A sufficiently large number of events were generated in each bin to obtain statistically significant samples after applying the selection criteria for the final states of interest.

As for the signal, the background events were simulated through the ATLFAST package, with pile-up effects included for the high-luminosity case. The b-tagging procedure and the jet energy recalibration were also applied. Table 5 shows the summed production cross-sections and the kinematical acceptances for selection S_{500} (before applying the b-tagging procedure), for the most prominent background

sub-processes: $b\bar{b}$, $q\bar{q}$, gb, gq and gg. The kinematical acceptances are about 0.13% for all the di-jet sub-processes, but the initial cross-sections vary over several orders of magnitude. Figure 5 shows the contributions from the various p_T bins chosen at generation to the distribution of $m_{b\bar{b}}$. The relative contributions from the different bins vary rapidly depending on the selection criteria, so the use of this algorithm for event generation turned out to be rather efficient in this case[3]. As an example, even though the production cross-sections in the first two bins are different by several orders of magnitude ($2 \cdot 10^7$ pb and $3.5 \cdot 10^4$ pb respectively), the contributions to the total background from these bins after selection S_{500} are comparable.

After selection, but before applying the b-tagging procedure, the inclusive background rates are approximately a factor of 10^4 to 10^5 higher than the signal rates in the mass bin of interest. Requiring at least three identified b-jets reduces this factor to 10^2 to 10^3. Requiring in addition a fourth identified b-jet gains another factor of about 2. In the sample containing at least three identified b-jets, approximately 40% of the background events contain at least three true b-jets, whereas in the sample containing at least four identified b-jets this fraction increases to 65%. These fractions can be estimated directly from the numbers shown in Table 6 by comparing the expected rates for an almost infinite rejection against non-b-jets ($R = 10^6$) with the default value of this rejection ($R = 10^2$).

The dominant remaining background arises from gb and gg production with gluon splitting into a $b\bar{b}$ pair. The contribution from direct $gg \to b\bar{b}$ production is found to be only at the level of $\sim 10\%$ of the total background. The contribution from $t\bar{t}$ production is very small ($\sim 1\%$). Figure 6 shows the respective contributions from the remaining background processes to the reconstructed $m_{b\bar{b}}$mass distribution, namely from direct $b\bar{b}$, from the summed $b\bar{b}$ + g b and from the summed all sub-processes, after applying the b-tagging procedure with the performance expected at high luminosity.

Table 5: *Production cross-sections and kinematical acceptances of the selection cuts described in Section 2.1, for various QCD background processes.*

Sub-process	σ (pb) $p_T^{gen} > 50$ GeV	Acceptance for selection S_{500}
$gg, qq \to gg, qq$	$1.32 \cdot 10^7$	0.12%
$gq \to gq$	$8.23 \cdot 10^6$	0.16%
$gb \to gb$	$4.40 \cdot 10^5$	0.15%
$gg, q\bar{q} \to q\bar{q}$	$4.32 \cdot 10^5$	0.15 %
$gg, q\bar{q} \to b\bar{b}$	$8.46 \cdot 10^4$	0.14%
$t\bar{t}$	$5.05 \cdot 10^2$	4.20%
Total	$2.22 \cdot 10^7$	0.13%

[3]Many thanks to F. Paige for this suggestion.

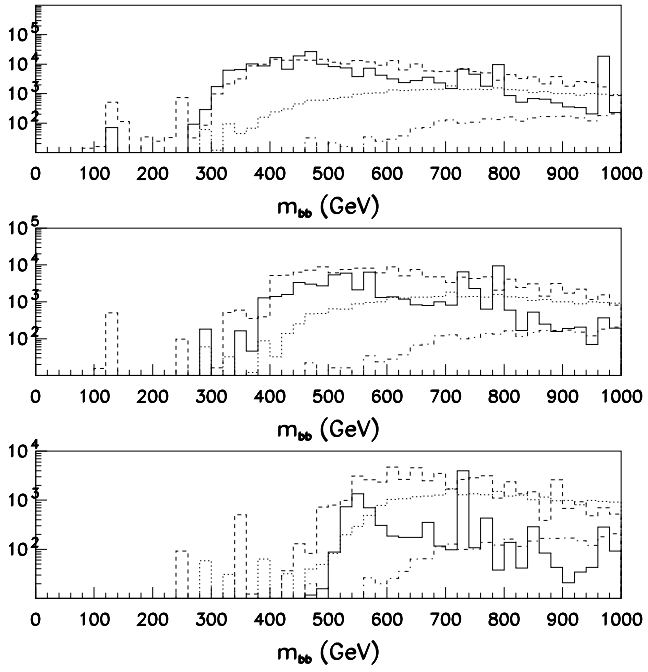

Figure 5: *Distribution of the reconstructed* $\mathrm{m_{b\bar{b}}}$ *mass for background events after applying the selection cuts* $\mathrm{S_{500}}$ *(top),* $\mathrm{S_{700}}$ *(middle) and* $\mathrm{S_{900}}$ *(bottom), for an integrated luminosity of* $3 \cdot 10^5$ *pb*$^{-1}$ *(ATLAS). The contributions from the different* $\mathrm{p_T}$ *bins used at generation are shown separately:* $50 < \mathrm{p_T}^{\mathrm{gen}} < 200$ *GeV (solid),* $200 < \mathrm{p_T}^{\mathrm{gen}} < 350$ *GeV (dashed),* $350 < \mathrm{p_T}^{\mathrm{gen}} < 500$ *GeV (dots), and* $\mathrm{p_T}^{\mathrm{gen}} > 500$ *GeV (dot-dashed).*

The background estimates presented above explain why the theoretical estimates of [8] are much too optimistic. These estimates were based on an evaluation of the QCD background in final states containing three b-jets using only the contribution from the direct $\mathrm{gg} \rightarrow \mathrm{b\bar{b}}$ sub-process. As appears clearly in Table 6, this sub-process contributes not more than 10 to 15% of the total background for final states containing at least three identified b-jets. This conclusion was found to be rather independent of the selection cuts applied to the reconstructed jets, as demonstrated by the results of Section 3.1 in Table 12.

Finally, Table 7 shows the total expected background for the different selection cuts, before and after applying the chosen $\mathrm{m_{b\bar{b}}}$ window, for an integrated luminosity of $3 \cdot 10^5$ pb^{-1} and the ATLAS experiment.

Table 6: *Expected rates of reconstructed background events after selection* S_{500} *as a function of the b-tagging performance, for an integrated luminosity of* $3 \cdot 10^5$ pb^{-1} *(ATLAS).*

Sub-process Selection S_{500}	Four jets	Jet1 tagged as b-jet	+ jet2 tagged as b-jet	+ jet3 tagged as b-jet	Algorithm A	Algorithm B
		$\epsilon_{\mathrm{b}} = 0.5, \quad \epsilon_{\mathrm{c}} = 10^{-6}, \quad \mathrm{R} = 10^6$				
$\mathrm{gg}, \mathrm{q\bar{q}} \to \mathrm{b\bar{b}}$	$3.5 \cdot 10^7$	$1.4 \cdot 10^7$	$3.7 \cdot 10^6$	$7.2 \cdot 10^4$	$7.3 \cdot 10^3$	$1.5 \cdot 10^4$
$\mathrm{gg}, \mathrm{q\bar{q}} \to \mathrm{q\bar{q}}$	$2.0 \cdot 10^8$	$1.6 \cdot 10^7$	$5.2 \cdot 10^6$	$3.7 \cdot 10^4$	$3.9 \cdot 10^3$	$1.0 \cdot 10^4$
$\mathrm{gb} \to \mathrm{gb}$	$1.8 \cdot 10^8$	$4.5 \cdot 10^7$	$4.2 \cdot 10^6$	$2.3 \cdot 10^5$	$2.2 \cdot 10^4$	$4.1 \cdot 10^4$
$\mathrm{gq} \to \mathrm{gq}$	$3.9 \cdot 10^9$	$3.5 \cdot 10^7$	$5.5 \cdot 10^5$	$2.2 \cdot 10^4$	$1.0 \cdot 10^2$	$8.4 \cdot 10^2$
$\mathrm{gg}, \mathrm{qq} \to \mathrm{gg}, \mathrm{qq}$	$4.8 \cdot 10^9$	$8.2 \cdot 10^7$	$4.6 \cdot 10^6$	$1.8 \cdot 10^5$	$1.4 \cdot 10^4$	$5.2 \cdot 10^4$
Total	$9.1 \cdot 10^9$	$1.9 \cdot 10^8$	$1.8 \cdot 10^7$	$5.4 \cdot 10^5$	$4.7 \cdot 10^4$	$1.2 \cdot 10^5$
		$\epsilon_{\mathrm{b}} = 0.5, \quad \epsilon_{\mathrm{c}} = 0.1, \quad \mathrm{R} = 10^2$				
$\mathrm{gg}, \mathrm{q\bar{q}} \to \mathrm{b\bar{b}}$	$3.5 \cdot 10^7$	$1.4 \cdot 10^7$	$3.9 \cdot 10^6$	$1.5 \cdot 10^5$	$1.0 \cdot 10^4$	$1.9 \cdot 10^4$
$\mathrm{gg}, \mathrm{q\bar{q}} \to \mathrm{q\bar{q}}$	$2.0 \cdot 10^8$	$2.0 \cdot 10^7$	$5.4 \cdot 10^6$	$1.2 \cdot 10^5$	$6.1 \cdot 10^3$	$1.5 \cdot 10^4$
$\mathrm{gb} \to \mathrm{gb}$	$1.8 \cdot 10^8$	$4.6 \cdot 10^7$	$5.1 \cdot 10^6$	$3.9 \cdot 10^5$	$3.1 \cdot 10^4$	$5.5 \cdot 10^4$
$\mathrm{gq} \to \mathrm{gq}$	$3.9 \cdot 10^9$	$9.2 \cdot 10^7$	$2.7 \cdot 10^6$	$1.3 \cdot 10^5$	$7.0 \cdot 10^3$	$1.3 \cdot 10^4$
$\mathrm{gg}, \mathrm{qq} \to \mathrm{gg}, \mathrm{qq}$	$4.8 \cdot 10^9$	$1.5 \cdot 10^8$	$7.8 \cdot 10^6$	$5.0 \cdot 10^5$	$2.8 \cdot 10^4$	$7.8 \cdot 10^4$
Total	$9.1 \cdot 10^9$	$3.2 \cdot 10^8$	$2.5 \cdot 10^7$	$1.3 \cdot 10^6$	$8.2 \cdot 10^4$	$1.8 \cdot 10^5$
		$\epsilon_b = 0.6, \quad \epsilon_c = 0.1, \quad \mathrm{R} = 10^2$				
$\mathrm{gg}, \mathrm{q\bar{q}} \to \mathrm{b\bar{b}}$	$3.5 \cdot 10^7$	$1.7 \cdot 10^7$	$5.5 \cdot 10^6$	$2.3 \cdot 10^5$	$2.0 \cdot 10^4$	$3.7 \cdot 10^4$
$\mathrm{gg}, \mathrm{q\bar{q}} \to \mathrm{q\bar{q}}$	$2.0 \cdot 10^8$	$2.3 \cdot 10^7$	$7.7 \cdot 10^6$	$1.8 \cdot 10^5$	$1.1 \cdot 10^4$	$2.8 \cdot 10^4$
$\mathrm{gb} \to \mathrm{gb}$	$1.8 \cdot 10^8$	$5.5 \cdot 10^7$	$7.1 \cdot 10^6$	$6.3 \cdot 10^5$	$6.1 \cdot 10^4$	$1.1 \cdot 10^5$
$\mathrm{gq} \to \mathrm{gq}$	$3.9 \cdot 10^9$	$9.9 \cdot 10^7$	$3.2 \cdot 10^6$	$1.9 \cdot 10^5$	$1.1 \cdot 10^4$	$2.0 \cdot 10^4$
$\mathrm{gg}, \mathrm{qq} \to \mathrm{gg}, \mathrm{qq}$	$4.8 \cdot 10^9$	$1.7 \cdot 10^8$	$1.0 \cdot 10^7$	$7.5 \cdot 10^5$	$5.0 \cdot 10^4$	$1.5 \cdot 10^5$
Total	$9.1 \cdot 10^9$	$3.6 \cdot 10^8$	$3.4 \cdot 10^7$	$2.0 \cdot 10^6$	$1.5 \cdot 10^5$	$3.4 \cdot 10^5$

Table 7: *Expected rates of reconstructed background events after applying the appropriate selection criteria, for an integrated luminosity of* $3 \cdot 10^5$ pb^{-1} *(ATLAS). The numbers of events accepted within the chosen* $\mathrm{m}_{\mathrm{b\bar{b}}}$ *mass window are shown in brackets.*

	Kinematical cuts	Three b-jets	Algorithm A	Algorithm B
Selection S_{500}	$9.2 \cdot 10^9$	$1.3 \cdot 10^6$ $(3.9 \cdot 10^5)$	$8.2 \cdot 10^4$ $(3.3 \cdot 10^4)$	$1.8 \cdot 10^5$ $(6.0 \cdot 10^4)$
Selection S_{700}	$5.1 \cdot 10^9$	$7.2 \cdot 10^5$ $(1.7 \cdot 10^5)$	$4.0 \cdot 10^4$ $(1.0 \cdot 10^4)$	$1.2 \cdot 10^5$ $(2.7 \cdot 10^4)$
Selection S_{900}	$2.0 \cdot 10^9$	$2.9 \cdot 10^5$ $(4.8 \cdot 10^4)$	$1.8 \cdot 10^4$ $(2.8 \cdot 10^3)$	$3.0 \cdot 10^4$ $(5.2 \cdot 10^3)$

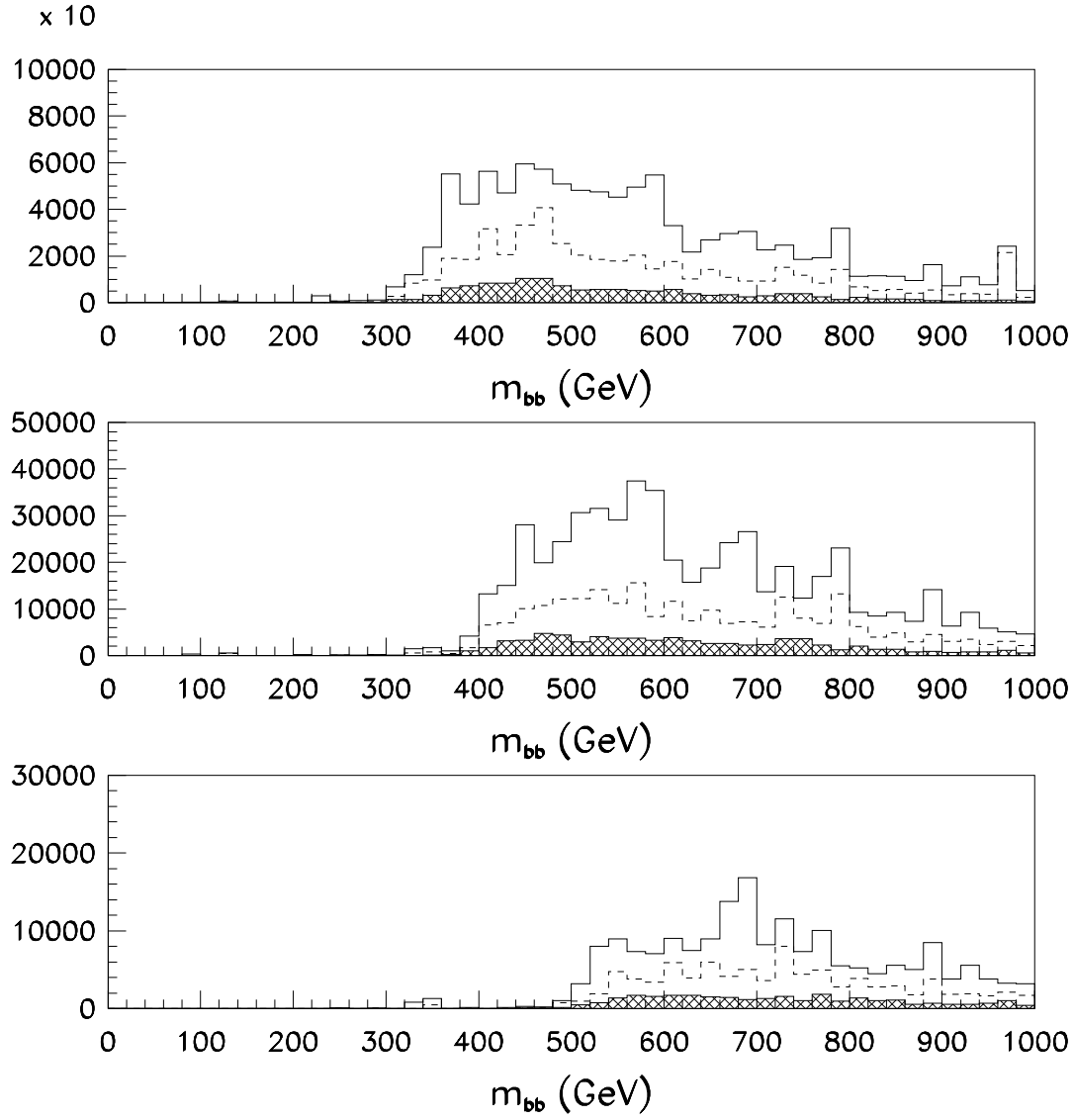

Figure 6: *Distribution of the reconstructed* $\mathrm{m_{b\bar{b}}}$ *mass for background events after applying the selection cuts* $\mathrm{S_{500}}$ *(top),* $\mathrm{S_{700}}$ *(middle) and* $\mathrm{S_{900}}$ *(bottom) and the b-tagging procedure, for an integrated luminosity of* $3 \cdot 10^5$ pb^{-1} *(ATLAS). The separate contributions from direct* $\mathrm{b\bar{b}}$ *(hashed), from* $\mathrm{b\bar{b}}$ + gb *(dashed) and the total spectrum (solid) are also shown.*

2.3 Expected signal significances

Table 8 (for an integrated luminosity of $3 \cdot 10^4$ pb^{-1}) and Table 9 (for an integrated luminosity of $3 \cdot 10^5$ pb^{-1}) show the final signal and background rates and expected significances for ATLAS experiment as a function of the selection procedure adopted, for $\tan\beta = 30$ and for four values of the Higgs-boson masses. The selection criteria (S_{300} to S_{900}), as well as the mass window for the reconstructed $m_{b\bar{b}}$, were optimised separately for each mass (a mass window of $\sim \pm 2\sigma_m$ was used).

The overall conclusion is that, even for an integrated luminosity of $3 \cdot 10^5$ pb^{-1}, the extraction of the signal for $b\bar{b}H/A$ production with $H/A \rightarrow b\bar{b}$ decay will be very difficult. Although the expected rates and significances are higher for a selection requiring only three identified b-jets, it is unlikely that the systematic uncertainties on the background shape can be controlled to the required precision in this case, where the signal-to-background ratio is lowest ($S/B \sim 1\%$). A selection requiring at least four identified b-jets yields a more favourable signal-to-background ratio of $\sim 3\%$ and also a more favourable ratio (of $\sim 67\%$) of irreducible-to-total background[4]. As mentioned previously, this latter ratio can be easily extracted from the numbers given in Table 6 for $R = 10^6$ and $R = 10^2$.

For a selection requiring four identified b-jets and for an integrated luminosity of $3 \cdot 10^5$ pb^{-1} (ATLAS), a nominal significance larger than 5σ could be achieved for $\tan\beta > 29$ ($m_H = 500$ GeV) and for $\tan\beta > 20$ ($m_H = 300$ GeV). This coverage in the parameter space can be compared with that of the $\tau\tau$ channel, which extends down to $\tan\beta > 25$ ($m_H = 500$ GeV) and to $\tan\beta > 8$ ($m_H = 300$ GeV). For an integrated luminosity of $3 \cdot 10^4$ pb^{-1}, the respective lower limits on $\tan\beta$ are $\tan\beta > 42$ and $\tan\beta > 30$ for the $b\bar{b}$ channel, and $\tan\beta > 33$ and $\tan\beta > 11$ for the $\tau\tau$ channel.

It should be stressed again that the sensitivities quoted for the $b\bar{b}$ channel are rather on the optimistic side, since the estimates of the QCD background are very uncertain (the PYTHIA results could be under-estimated by a factor of 3), and the assumptions used for the b-tagging performance are more optimistic than the results from recent work for the ATLAS Inner Detector Performance TDR [13]. In addition, systematic uncertainties due to the lack of knowledge of the background shape have not been taken into account in the significance estimates of Tables 8 and 9.

[4]The irreducible background consists of the events containing the required number of identified true b-jets.

Table 8: *Expected signal and background rates inside the* $m_{b\bar{b}}$ *mass window, for four values of* m_H *and* m_A*, for* $\tan\beta = 30$ *and for an integrated luminosity of* $3 \cdot 10^4$ pb^{-1} *(ATLAS). Also shown are the expected signal-to-background ratios and signal significances for various selection algorithms (see text).*

$b\bar{b}H/A$ with $H/A \to b\bar{b}$	Signal (S)	Background (B)	S/B	$S/\sqrt{B}$
	$m_H = 300$ GeV			
Selection S_{300}				
Three b-jets	3200	$2.1 \cdot 10^5$	1.5%	7.0
Algorithm A	630	$2.4 \cdot 10^4$	2.6%	4.1
Algorithm B	1075	$4.6 \cdot 10^4$	2.3%	5.0
	$m_H = 500$ GeV			
Selection S_{500}				
Three b-jets	855	$5.9 \cdot 10^4$	1.4%	3.5
Algorithm A	200	$6.1 \cdot 10^3$	3.3%	2.6
Algorithm B	265	$1.1 \cdot 10^4$	2.4%	2.5
	$m_H = 700$ GeV			
Selection S_{700}				
Three b-jets	260	$2.6 \cdot 10^4$	1.0%	1.6
Algorithm A	50	$1.8 \cdot 10^3$	2.8%	1.2
Algorithm B	70	$5.1 \cdot 10^3$	1.4%	1.0
	$m_H = 900$ GeV			
Selection S_{900}				
Three b-jets	90	$7.3 \cdot 10^3$	1.2%	1.0
Algorithm A	16	$5.2 \cdot 10^2$	3.0%	0.7
Algorithm B	25	$9.9 \cdot 10^2$	2.5%	0.8

Table 9: *Expected signal and background rates inside the* $m_{b\bar{b}}$ *mass window, for four values of* m_H *and* m_A*, for* $\tan\beta = 30$ *and for an integrated luminosity of* $3 \cdot 10^5$ pb^{-1} *(ATLAS). Also shown are the expected signal-to-background ratios and signal significances for various selection algorithms (see text).*

$b\bar{b}H/A$ with $H/A \to b\bar{b}$	Signal (S)	Background (B)	S/B	$S/\sqrt{B}$
	$m_H = 300$ GeV			
Selection S_{300}				
Three b-jets	18700	$1.4 \cdot 10^6$	1.3%	15.8
Algorithm A	3080	$1.3 \cdot 10^5$	2.4%	8.5
Algorithm B	5270	$2.4 \cdot 10^5$	2.2%	10.7
	$m_H = 500$ GeV			
Selection S_{500}				
Three b-jets	5000	$3.9 \cdot 10^5$	1.3%	8.0
Algorithm A	960	$3.3 \cdot 10^4$	2.9%	5.3
Algorithm B	1300	$6.0 \cdot 10^4$	2.2%	5.3
	$m_H = 700$ GeV			
Selection S_{900}				
Three b-jets	1530	$1.7 \cdot 10^5$	0.9%	3.7
Algorithm A	240	$1.0 \cdot 10^4$	2.4%	2.4
Algorithm B	350	$2.7 \cdot 10^4$	1.3%	2.1
	$m_H = 900$ GeV			
Selection S_{900}				
Three b-jets	524	$4.8 \cdot 10^4$	1.1%	2.4
Algorithm A	80	$2.8 \cdot 10^3$	2.8%	1.5
Algorithm B	122	$5.2 \cdot 10^3$	2.3%	1.7

3 Observability of $H \rightarrow hh \rightarrow b\bar{b}b\bar{b}$ for small $\tan\beta$

3.1 Signal events

Two points in the MSSM parameter space were chosen for a detailed study of this channel: $m_H = 300$ GeV with $\tan\beta = 1.5$ and $\tan\beta = 3.0$, corresponding respectively to $m_h = 77.8$ GeV and $m_h = 98$ GeV (2-loop calculation). The final state in this channel can be fully reconstructed with good mass resolution through the use of the constraint, $m_{b\bar{b}} = m_h$. Four identified b-jets are required with two $b\bar{b}$ combinations reconstructed with $m_{b\bar{b}}$ close to m_h. As shown also in [14], with the expected ATLAS calorimeter performance, a signal acceptance of 70% to 80% can be achieved using a mass window, $m_{b\bar{b}} = m_h \pm 25$ GeV, for the h-boson reconstruction and, after applying the constraint on m_h, a mass window, $m_{b\bar{b}b\bar{b}} = m_H \pm 20$ GeV.

For the signal events, the jet transverse-energy spectrum is rather hard, with $< {p_T}^{j_1} > = 100$ GeV and $< {p_T}^{j_4} > = 36$ GeV for jets within the Inner Detector acceptance for b-tagging. For the high-luminosity case, at least four jets reconstructed with $p_T > 40$ GeV (before energy recalibration) are required, yielding an acceptance of $\sim 25\%$ for the signal events. Table 10 shows the expected signal rates for two different jet-selection algorithms described below:

- Algorithm A:
  - the four most energetic jets are required to be identified as b-jets;
  - all possible $b\bar{b}$ combinations are then reconstructed;
  - the best pair of combinations for the reconstruction of m_h is chosen by minimising $\chi^2 = (m_{b\bar{b},1} - m_h)^2 + (m_{b\bar{b},2} - m_h)^2$;
  - both pairs are required to satisfy $m_{b\bar{b}} = m_h \pm 25$ GeV;
  - the event is accepted if $m_{b\bar{b}b\bar{b}} = m_H \pm 20$ GeV after applying a constraint on m_h.
- Algorithm B:
  - all possible jj combinations inside the Inner Detector acceptance are considered;
  - the best pair of combinations for the reconstruction of m_h is chosen by minimising $\chi^2 = (m_{jj,1} - m_h)^2 + (m_{jj,2} - m_h)^2$;
  - all four jets chosen in this way are required to be identified as b-jets;
  - both pairs are required to satisfy $m_{b\bar{b}} = m_h \pm 25$ GeV;
  - the event is accepted if $m_{b\bar{b}b\bar{b}} = m_H \pm 20$ GeV after applying a constraint on m_h.

A careful comparison of these algorithms with other possible selection methods has shown that Algorithm B is close to optimal.

Table 10: *Numbers of expected* $H \to hh \to b\bar{b}b\bar{b}$ *signal events as a function of the selection algorithm, for an integrated luminosity of* $3 \cdot 10^5$ pb^{-1} *(ATLAS). The high-luminosity b-tagging performance is assumed (*$\epsilon_b = 50\%$, $\epsilon_c = 10\%$ *and* $R = 100$*).*

$m_H = 300$ GeV	σ (pb)	Four reconstructed jets	Four identified b-jets	+ $m_{b\bar{b}}$ within ± 25 GeV of m_h	+ m_H within ± 20 GeV of m_H.
			Algorithm A		
$\tan\beta = 3.0$	0.76	$5.8 \cdot 10^4$	350	154	125
$\tan\beta = 1.5$	1.73	$1.6 \cdot 10^5$	800	510	430
			Algorithm B		
$\tan\beta = 3.0$	0.76	$5.8 \cdot 10^4$	640	470	360
$\tan\beta = 1.5$	1.73	$1.6 \cdot 10^5$	1760	1560	1360

3.2 Background events

As in Section 2.2, the background events arise dominantly from QCD multi-jet production. Table 11 shows the expected rates of reconstructed multi-jet background events for the various QCD sub-processes and for an integrated luminosity of $3 \cdot 10^5$ pb^{-1}. This Table also shows the contributions from events containing one or more true b-jets to each of the sub-processes; for the dominant gg sub-process, only 0.01% of the events contain four true b-jets in the final state, whereas this factor increases to 0.8% for the direct $b\bar{b}$ sub-process. Nevertheless, since the production cross-sections differ by two orders of magnitude, the direct $b\bar{b}$ production process contributes only $\sim 10\%$ of the total QCD background after having required four tagged b-jets, as shown in Table 12. The dominant background is from the gb sub-process, and the irreducible background from four true b-jets is shown to amount to $\sim 70\%$ of the total multi-jet background. This can be deduced from a comparison of the expected background rates in Table 12 for $R = 10^6$ (almost infinite rejection of non-b-jets) and for $R = 10^2$ (default b-tagging performance). This is also illustrated in Fig. 7, which displays the mass distributions expected for the candidate $h \to b\bar{b}$ decays for the three dominant sub-processes and for the events accepted by algorithm B. Finally, Table 13 shows the expected rates of background events at each step of the selection procedures described as Algorithms A and B.

Table 11: *Expected rates of QCD multi-jet background events for different sub-processes and for an integrated luminosity of* $3 \cdot 10^5$ pb^{-1} *(ATLAS). Also shown are the contributions to the total background from events containing one or more true b-jets.*

Sub-process	Four jets with $p_T > 40$ GeV and $\|\eta\| < 2.5$	Jet1 = true b-jet	+ jet2 = true b-jet	+ jet3 = true b-jet	+ jet4 = true b-jet
$gg, q\bar{q} \to b\bar{b}$	$2.0 \cdot 10^8$	70%	30%	2%	0.8%
$gb \to gb$	$1.2 \cdot 10^9$	45%	10%	1%	0.3%
$gg, qq \to gg, qq$	$1.7 \cdot 10^{10}$	3%	0.4%	0.04%	0.01%

Table 12: *Expected rates of reconstructed background events after jet-selection cuts as a function of the b-tagging performance, for an integrated luminosity of* $3 \cdot 10^5$ pb^{-1} *(ATLAS).*

Sub-process	Four jets with $p_T > 40$ GeV and $\|\eta\| < 2.5$	Jet1 tagged as b-jet	+ jet2 tagged as b-jet	+ jet3 tagged as b-jet	+jet4 tagged as b-jet
		$\epsilon_b = 0.5$, $\epsilon_c = 10^{-6}$, R = 10^6			
$gg, q\bar{q} \to b\bar{b}$	$2.0 \cdot 10^8$	$6.9 \cdot 10^7$	$1.5 \cdot 10^7$	$5.0 \cdot 10^5$	$9.7 \cdot 10^4$
$gb \to gb$	$1.2 \cdot 10^9$	$2.7 \cdot 10^8$	$2.9 \cdot 10^7$	$1.5 \cdot 10^6$	$2.1 \cdot 10^5$
$gg, qq \to gg, qq$	$1.7 \cdot 10^{10}$	$2.6 \cdot 10^8$	$1.6 \cdot 10^7$	$8.6 \cdot 10^5$	$1.2 \cdot 10^5$
Total	$1.8 \cdot 10^{10}$	$6.0 \cdot 10^8$	$6.0 \cdot 10^7$	$2.9 \cdot 10^6$	$4.3 \cdot 10^5$
		$\epsilon_b = 0.5$, $\epsilon_c = 0.1$, R = 10^2			
$gg, q\bar{q} \to b\bar{b}$	$2.0 \cdot 10^8$	$7.0 \cdot 10^7$	$1.6 \cdot 10^7$	$9.5 \cdot 10^5$	$1.2 \cdot 10^5$
$gb \to gb$	$1.2 \cdot 10^9$	$2.8 \cdot 10^8$	$3.4 \cdot 10^7$	$2.6 \cdot 10^6$	$2.9 \cdot 10^5$
$gg, qq \to gg, qq$	$1.7 \cdot 10^{10}$	$5.2 \cdot 10^8$	$2.8 \cdot 10^7$	$2.1 \cdot 10^6$	$1.9 \cdot 10^5$
Total	$1.8 \cdot 10^{10}$	$8.7 \cdot 10^8$	$7.8 \cdot 10^7$	$5.6 \cdot 10^6$	$6.0 \cdot 10^5$
		$\epsilon_b = 0.6$, $\epsilon_c = 0.1$, R = 10^2			
$gg, q\bar{q} \to b\bar{b}$	$2.0 \cdot 10^8$	$8.4 \cdot 10^7$	$2.2 \cdot 10^7$	$1.5 \cdot 10^6$	$2.4 \cdot 10^5$
$gb \to gb$	$1.2 \cdot 10^9$	$3.3 \cdot 10^8$	$4.8 \cdot 10^7$	$4.2 \cdot 10^6$	$5.6 \cdot 10^5$
$gg, qq \to gg, qq$	$1.7 \cdot 10^{10}$	$5.7 \cdot 10^8$	$3.6 \cdot 10^7$	$3.2 \cdot 10^6$	$3.5 \cdot 10^5$
Total	$1.8 \cdot 10^{10}$	$9.8 \cdot 10^8$	$1.1 \cdot 10^8$	$8.9 \cdot 10^6$	$1.1 \cdot 10^6$

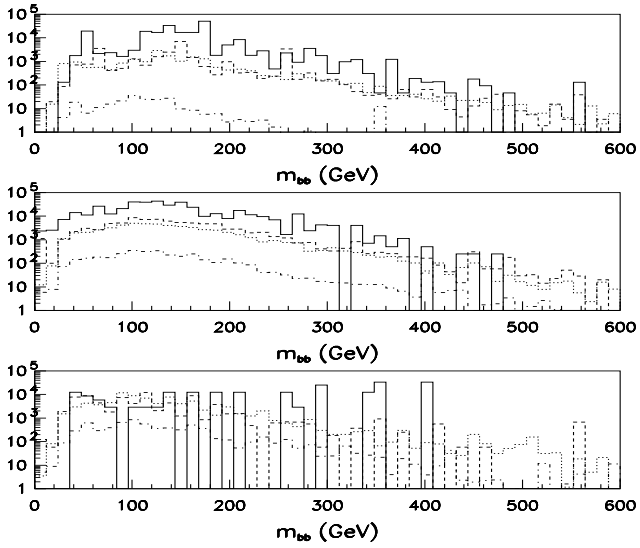

Figure 7: *Distribution of the reconstructed* $\mathrm{m_{b\bar{b}}}$ *for background events after applying selection B, shown separately for the various sub-processes:* $\mathrm{b\bar{b}}$ *(top), gb (middle) and* $\mathrm{gg + gq + qq}$ *(bottom). Also shown separately are the contributions from events containing four true b-jets (solid), three true b-jets (dashed), two true b-jets (dots) and one or less true b-jets (dot-dashed).*

Table 13: *Expected rates of reconstructed background events as a function of the selection cuts, for algorithms A and B and for an integrated luminosity of* $3 \cdot 10^5$ pb^{-1} *(ATLAS). The default high luminosity b-tagging performance is assumed.*

Sub-process	σ (mb) $\mathrm{p_T} > 10$ GeV	Four jets with $\mathrm{p_T} > 40$ GeV and $\lvert\eta\rvert < 2.5$	Four jets identified as b-jets	$\mathrm{m_h}$ within $\pm$ 25 GeV of nominal	$\mathrm{m_H}$ within $\pm$ 20 GeV of nominal
			Algorithm A		
bb	$2.1 \cdot 10^{-3}$	$2.0 \cdot 10^8$	$1.2 \cdot 10^5$	2000	200
gb	$7.1 \cdot 10^{-2}$	$1.2 \cdot 10^9$	$2.8 \cdot 10^5$	13000	1900
gg, gq, qq	5.9	$1.7 \cdot 10^{10}$	$1.9 \cdot 10^5$	2000	500
Total		$1.8 \cdot 10^{10}$	$5.9 \cdot 10^5$	17000	2600
			Algorithm B		
bb	$2.1 \cdot 10^{-3}$	$2.0 \cdot 10^8$	$1.4 \cdot 10^5$	3000	500
gb	$7.1 \cdot 10^{-2}$	$1.2 \cdot 10^9$	$2.9 \cdot 10^5$	24000	2500
gg, gq, qq	5.9	$1.7 \cdot 10^{10}$	$1.9 \cdot 10^5$	14000	1000
Total		$1.8 \cdot 10^{10}$	$6.2 \cdot 10^5$	41000	4000

3.3 Significance

Table 14 shows, for both algorithms A and B, the expected signal and background rates for $m_H = 300$ GeV, for $\tan\beta$ =1.5 and 3.0, and for an integrated luminosity of $3 \cdot 10^5$ pb^{-1}. Algorithm B yields a significantly better signal-to-background ratio and thereby sensitivity, since b-jets from $H \to hh \to b\bar{b}b\bar{b}$ decays are not very often the hardest jets in the event.

The $m_{b\bar{b}}$ and $m_{b\bar{b}b\bar{b}}$ mass distributions for both the signal and background events selected by algorithm B are shown in Fig. 8 and Figure 9 before the relevant mass cuts are applied. Fig. 10 shows the distributions of $p_T^{b\bar{b}}$, $p_T^{b\bar{b}b\bar{b}}$, $p_T^{b_1}$ and $p_T^{b_4}$ before energy recalibration for the accepted signal and background events. After applying the selection cuts of algorithm B, these distributions do not differ sufficiently between signal and the background to justify further optimisation of the selection cuts.

A sensitivity similar to that expected for the $H \to hh \to b\bar{b}\gamma\gamma$ channel (see Fig. 2) appears to be also achievable in this channel, since rate is larger, but this would require triggering on four-jet events at high luminosity with $p_T^{jet} > 40$ GeV and $|\eta| < 2.5$. The expected trigger rates are very uncertain, in the range between 1.6 and 4.5 kHz for PYTHIA and NJETS respectively (before energy recalibration), and also too high to be accepted without further cuts at level-2. The possibility of using b-tagging to reduce the rate will be investigated and compared with other simpler possibilities involving somewhat tighter cuts.

This channel has also been studied in the low-luminosity case to evaluate the possible gain in sensitivity that could be achieved by lowering the jet E_T-threshold. The results of this study are shown, for algorithm B, for $\tan\beta = 3.0$ and for an integrated luminosity of $3 \cdot 10^4$ pb^{-1}, in Table 15 as a function of the jet E_T-threshold, which was varied from its minimum realistic value (before recalibration) of 15 GeV to the high-luminosity value of 40 GeV. The background rates decrease much faster than the signal rates and the sensitivity improves as the jet E_T-threshold is raised. For a threshold of 20 GeV, Fig. 11 shows the distributions of $p_T^{b\bar{b}}$, $p_T^{b\bar{b}b\bar{b}}$, $p_T^{b_1}$ and $p_T^{b_4}$ for the accepted signal and background events: requiring a cut on $p_T^{b\bar{b}}$, typically $p_T^{b\bar{b}} > 60$ GeV, would obviously improve the signal sensitivity. As an illustration, Table 15 also shows the resulting expected signal and background rates as well as the signal-to-background ratios and signal significances, for events with $p_T^{b\bar{b}} > 60$ GeV and with $p_T^{b_1} > 80$ GeV, as a function of the jet E_T-threshold.

Even with optimised cuts, the sensitivity at low luminosity is weaker than that for the $H \to hh \to b\bar{b}\gamma\gamma$ channel [5], and the trigger requirements become very demanding, since an E_T-threshold of about 20 GeV would be desirable.

Table 14: *For* $m_H = 300$ *GeV and two values of* $\tan\beta$*, expected signal and background rates, signal-to-background ratios and signal significances, for the two selection algorithms A and B described in the text and for an integrated luminosity of* $3 \cdot 10^5$ pb^{-1} *(ATLAS).*

$H \to hh \to b\bar{b}b\bar{b}$	σ(pb)	S	B	S/B	$S/\sqrt{B}$
		Algorithm A			
$\tan\beta = 3.0$	0.76	125	2600	4.8 %	2.4
$\tan\beta = 1.5$	1.73	430	2600	16.5 %	8.4
		Algorithm B			
$\tan\beta = 3.0$	0.76	360	4000	9.0 %	5.7
$\tan\beta = 1.5$	1.73	1360	4000	34.0 %	21.5

Table 15: *For* $m_H = 300$ *GeV and* $\tan\beta = 3.0$*, expected signal and background rates, signal-to-background ratios and signal significances as a function of the chosen jet* E_T*-threshold, for an integrated luminosity of* $3 \cdot 10^4$ pb^{-1} *(ATLAS).*

$H \to hh \to b\bar{b}b\bar{b}$	S	B	S/B	$S/\sqrt{B}$
Jet E_T threshold	Algorithm B			
15 GeV	275	64 000	0.4 %	1.1
20 GeV	231	48 000	0.5 %	1.1
30 GeV	132	10 000	1.3 %	1.3
40 GeV	50	800	6.2 %	1.8
	$+p_T^{bb} > 60$ GeV and $p_T^{b_1} > 80$ GeV			
15 GeV	160	3 900	4.1 %	2.6
20 GeV	132	2 500	5.3 %	2.6
30 GeV	75	1 500	5.0 %	1.9
40 GeV	30	400	7.5 %	1.5

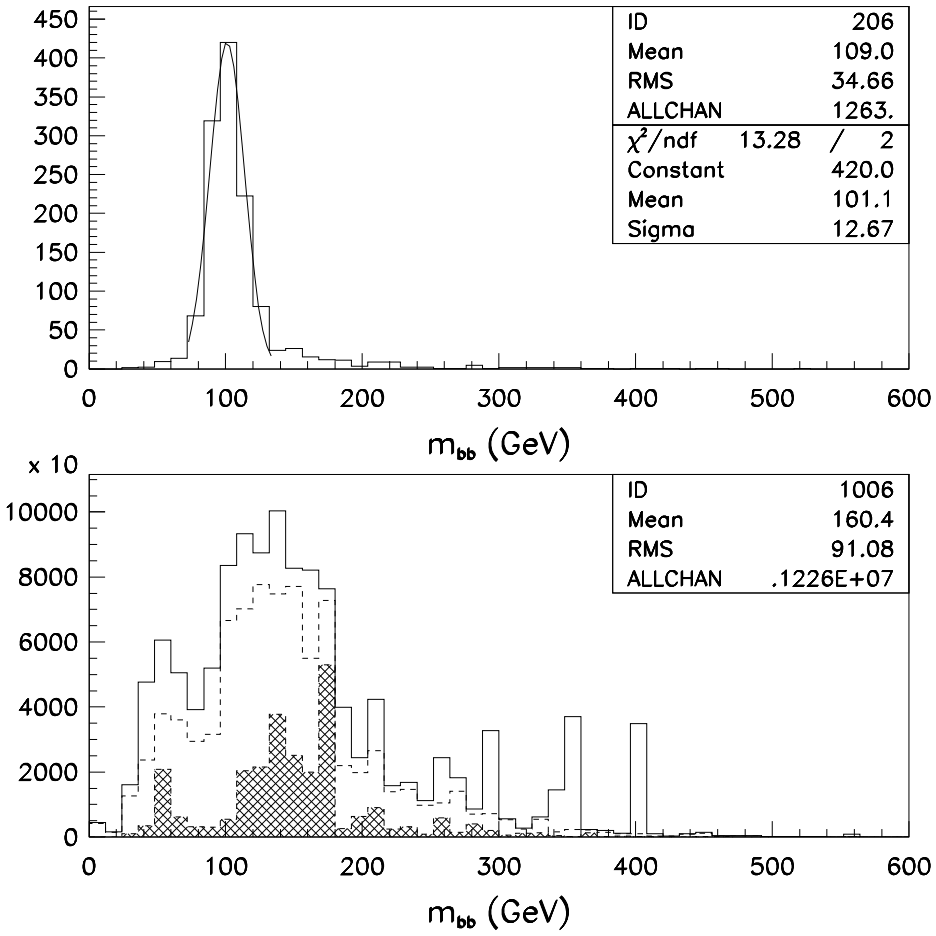

Figure 8: *Distribution of the reconstructed* $\mathrm{m_{b\bar{b}}}$ *mass for the two best combinations in events containing four b-jets selected by algorithm B and for an integrated luminosity of* $3 \cdot 10^5$ pb^{-1} *(ATLAS). The top distribution is for* $\mathrm{H \rightarrow hh \rightarrow b\bar{b}b\bar{b}}$ *signal events with* $\mathrm{m_H}$ *= 300 GeV and* $\tan\beta$ *= 1.5, corresponding to* $\mathrm{m_h}$ *= 98 GeV. The bottom distribution is for the background from multi-jet production (solid), where the contributions from direct* $\mathrm{b\bar{b}}$ *(cross-hatched) and* $\mathrm{b\bar{b} + gb}$ *production (dashed) are also shown.*

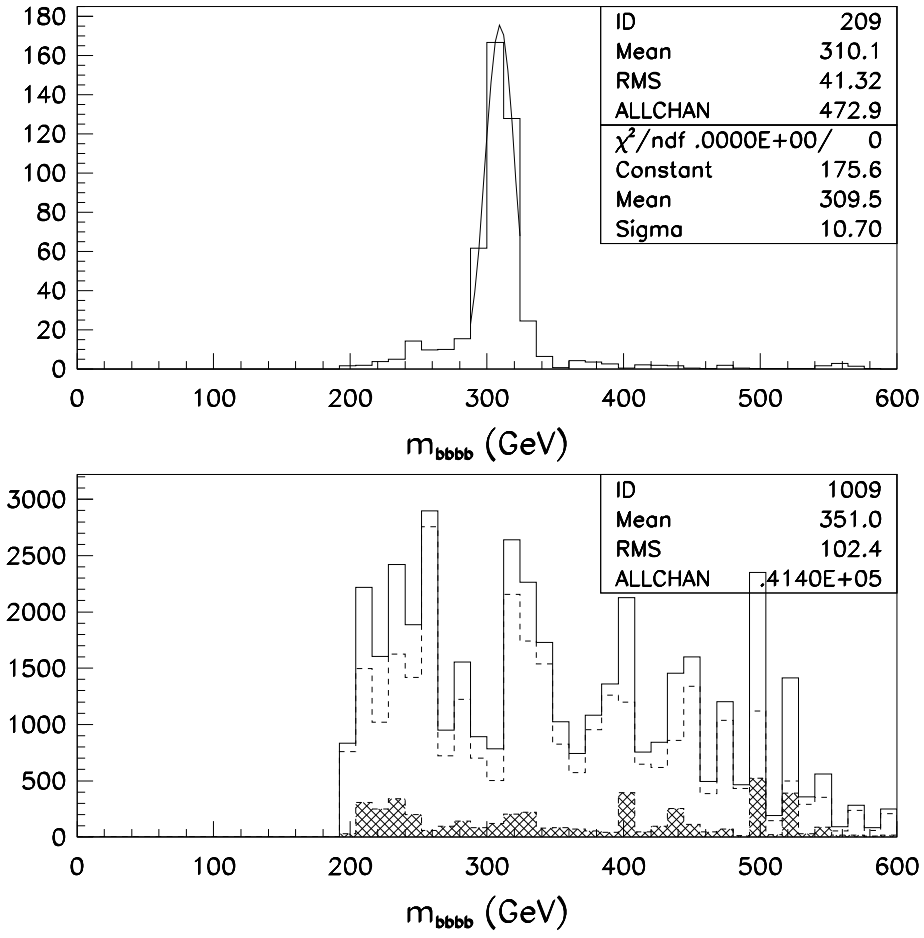

Figure 9: *Same as Fig. 8 for the* $\mathrm{m_{b\bar{b}b\bar{b}}}$ *spectrum after applying a constraint,* $\mathrm{m_{b\bar{b}}} = \mathrm{m_h}$, *on the two best* $b\bar{b}$ *combinations.*

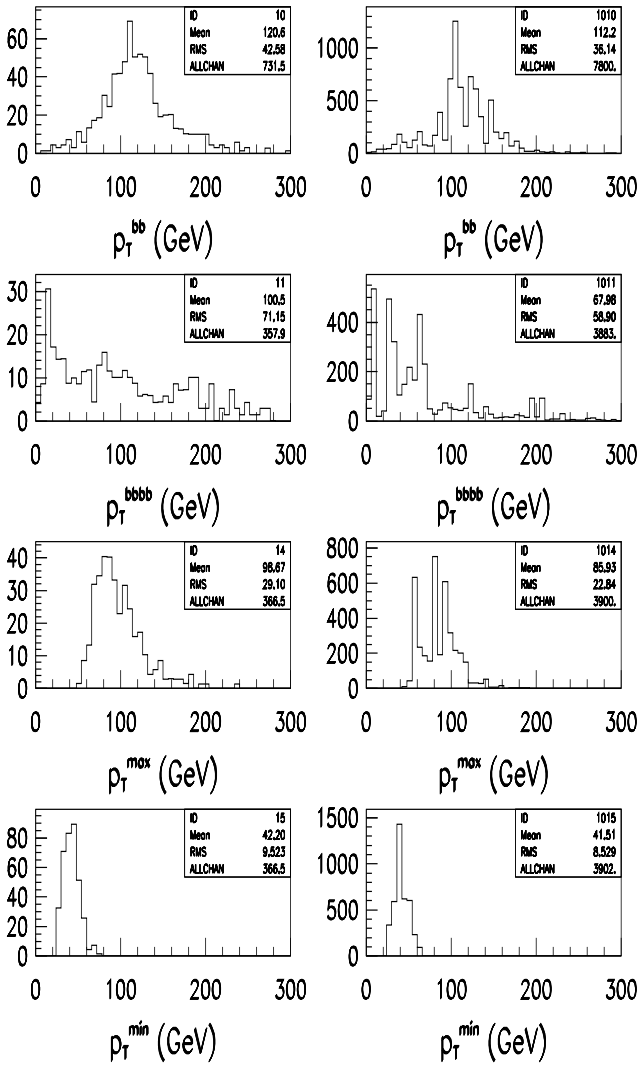

Figure 10: *Distributions of* $\mathrm{p_T^{b\bar{b}}}$, $\mathrm{p_T^{b\bar{b}b\bar{b}}}$, $\mathrm{p_T^{b_1}}$ *and* $\mathrm{p_T^{b_4}}$ *for signal (left) and background (right) after applying the selection B with a jet* $\mathrm{E_T}$*-threshold of 40 GeV, for an integrated luminosity of* $3 \cdot 10^5$ pb^{-1} *(ATLAS).*

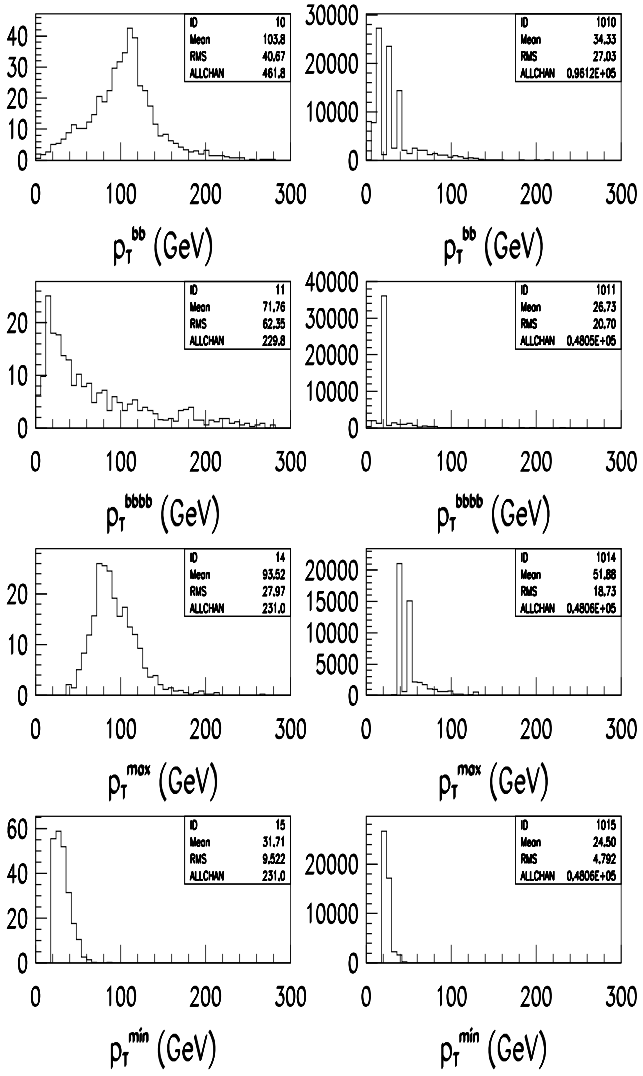

Figure 11: *Distributions of* $\mathrm{p_T^{b\bar{b}}}$, $\mathrm{p_T^{b\bar{b}b\bar{b}}}$, $\mathrm{p_T^{b_1}}$ *and* $\mathrm{p_T^{b_4}}$ *for signal (left) and background (right) after applying the selection B with a jet* $\mathrm{E_T}$*-threshold of 20 GeV, for an integrated luminosity of* $3 \cdot 10^4$ pb^{-1} *(ATLAS).*

4 Conclusions

This first study of event topologies containing four b-jets in the search for MSSM Higgs-boson decays has shown that it will be very difficult to cleanly extract the signal above the background over a significant region of the MSSM parameter space. The results of this note are much less optimistic than those from [8], because the study reported in [8] did not consider all processes leading to multiple b-jets in the final state, nor did it consider the significant fraction of fake b-jets to be expected in such complex topologies. The study reported here was particularly difficult to bring to a conclusion since more than $2 \cdot 10^7$ background events had to be generated and processed through ATLFAST.

The $b\bar{b}H$, $b\bar{b}A$ with $H, A \rightarrow b\bar{b}$ channel was considered for large values of m_H, m_A and $\tan\beta$. The strongly enhanced production cross-section of 3.5 pb for m_H=500 GeV and $\tan\beta = 30$ yields 10^6 signal events for an integrated luminosity of $3 \cdot 10^5$ pb^{-1}. This large rate is however strongly reduced by the selection cuts and the b-tagging efficiencies, leading to roughly 5000 observable events in a mass bin of $\pm$80 GeV around m_H, m_A. The QCD multi-jet background is initially several orders of magnitude higher and after the selection cuts and the b-tagging procedure a signal-to-background ratio of only a few percent can be achieved. The sensitivity to this channel is therefore rather weak.

The $H \rightarrow hh \rightarrow b\bar{b}b\bar{b}$ channel was studied for low $\tan\beta$ and $m_H = 300$ GeV. Fully reconstructed $h \rightarrow b\bar{b}$ and $H \rightarrow hh$ decays in relatively narrow mass windows would give firm evidence for both h and H Higgs boson production. But in the presence of the huge QCD background, the sensitivity to this channel is also weak, weaker than that of the $H \rightarrow hh \rightarrow bb\gamma\gamma$ channel.

In both cases, at most only a fraction of the MSSM parameter space, which is already covered by other decay modes ($b\bar{b}H$, $b\bar{b}A$, with $H, A \rightarrow \tau\tau$ and $H \rightarrow hh \rightarrow b\bar{b}\gamma\gamma$) is accessible to these channels containing four b-jets in the final state. Nevertheless, their observation would help in constraining the couplings and branching ratios of the MSSM Higgs bosons.

References

[1] H.P. Nilles, Phys. Rep. **110** (1984) 1; H.E. Haber and G.L. Kane, Phys. Rep.**117** (1985) 75; A.B. Lahanas and D.V. Nanopoulos, Phys. Rep. **145** (1987) 1; R. Barbieri, Riv. Nuovo Cimento **11** (1988) 1;

[2] for review on the Higgs sector in MSSM see J.F. Gunion, H.E. Haber, G.L. Kane and S. Dawson, The Higgs Hunter's Guide (Addison-Wesley, New York, 1990).

[3] M. Carena, P.M. Zerwas et al., in Physics at LEP2, Volume 1, edited by G. Altarelli, T. Sjöstrand, and F. Zwirner, CERN Yellow Report 96-01 (1996) pp.351-462.

[4] H.E. Haber and R. Hempfling, Phys. Rev. Lett. **66** (1991) 1815.

Y. Okada, M. Yamaguchi and T. Yanagida, prog. Theor. Phys. **85** (1991) 1; J. Ellis, G. Ridolfi and F. Zwirner, Phys. Lett. **B257** (1991) 83.

M. Carena, J.R. Espinosa, M. Quiros and C.E.M. Wagner, Phys. Lett. **355** (1995) 209; M. Carena, M. Quiros and C.E.M. Wagner, Nucl. Phys. **B461** (1996) 407.

[5] E. Richter-Was, D. Froidevaux, F. Gianotti, L. Poggioli, D. Cavalli and S. Resconi, CERN preprint, CERN-TH/96-111 (1996).

[6] ATLAS Collaboration, Technical Proposal, CERN/LHCC/94-43, December 1994.

CMS Collaboration, Technical proposal, CERN/LHCC/94-38, December 1994.

[7] D. Cavalli and S. Resconi, presentation on ATLAS week (March 1997).

[8] J. Dai, J. F. Gunion and R. Vega, Phys. Lett. **B345** (1995) 29, and update in preprint UCD-96-021 (July 1996).

[9] E. Richter-Was and D. Froidevaux, ATLAS Internal Note, PHYS-No-104 (1997).

[10] F.A. Berends and H. Kuijf, Nucl. Phys. **B353** (1991) 59.

[11] T. Sjöstrand, CERN preprint TH.7112/93; Comput. Phys. Commun. **39** (1986) 347;

T. Sjöstrand and M. Bengtsson, Comput. Phys. Commun. **43** (1987) 367.

[12] E. Richter-Was, D. Froidevaux and L. Poggioli, ATLAS Internal Note,
PHYS-No-079 (1996).

[13] ATLAS Collaboration, ATLAS Inner Detector Technical Design Report,
Volume 1, ATLAS TDR 4, CERN/LHCC/97-16 (30 April 1997).

[14] D. Froidevaux and E. Richter-Was, Z. Phys. **C67** (1995) 213.

[15] ATLAS Collaboration, ATLAS Calorimeter Performance, ATLAS TDR 1, CERN/LHCC/96-40 (15 December 1996).

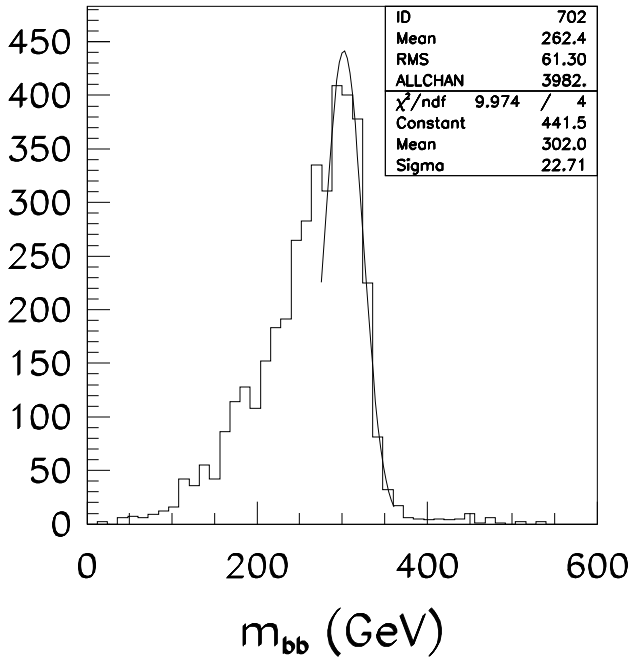
ID 702
Mean 262.4
RMS 61.30
ALLCHAN 3982.
χ²/ndf 9.974 / 4
Constant 441.5
Mean 302.0
Sigma 22.71
0 50 100 150 200 250 300 350 400 450
0 200 400 600
m_bb (GeV)

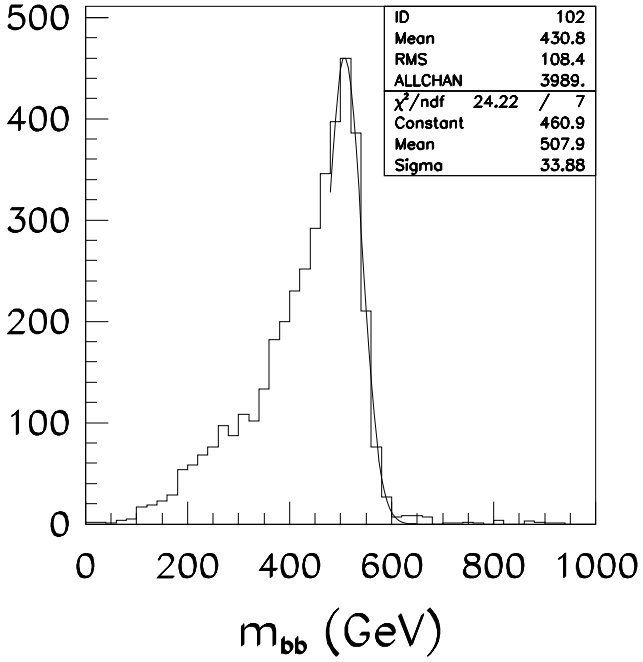
ID 102
Mean 430.8
RMS 108.4
ALLCHAN 3989.
χ²/ndf 24.22 / 7
Constant 460.9
Mean 507.9
Sigma 33.88
0 100 200 300 400 500
0 200 400 600 800 1000
m_bb (GeV)

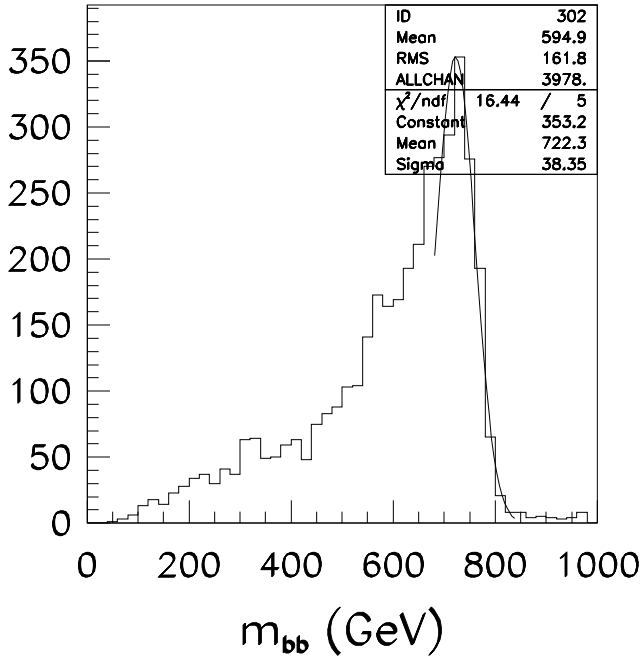
ID 302
Mean 594.9
RMS 161.8
ALLCHAN 3978.
χ²/ndf 16.44 / 5
Constant 353.2
Mean 722.3
Sigma 38.35
0 50 100 150 200 250 300 350
0 200 400 600 800 1000
m_bb (GeV)

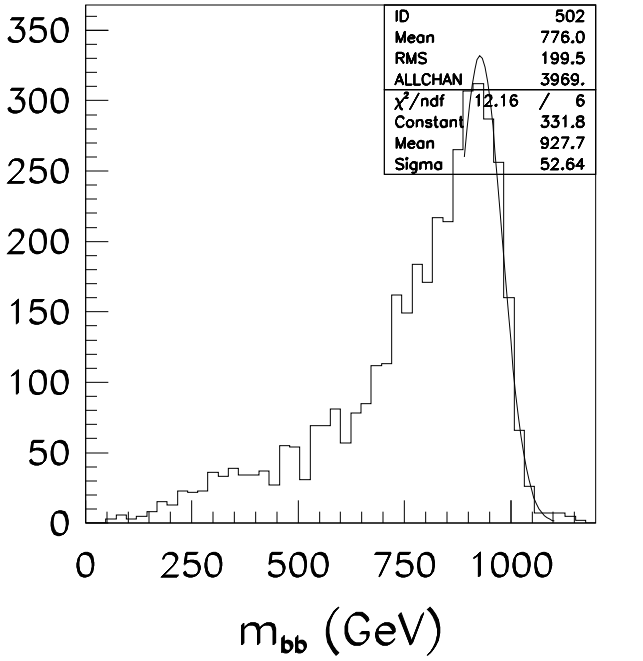
ID 502
Mean 776.0
RMS 199.5
ALLCHAN 3969.
χ²/ndf 12.16 / 6
Constant 331.8
Mean 927.7
Sigma 52.64
0 50 100 150 200 250 300 350
0 250 500 750 1000
m_bb (GeV)

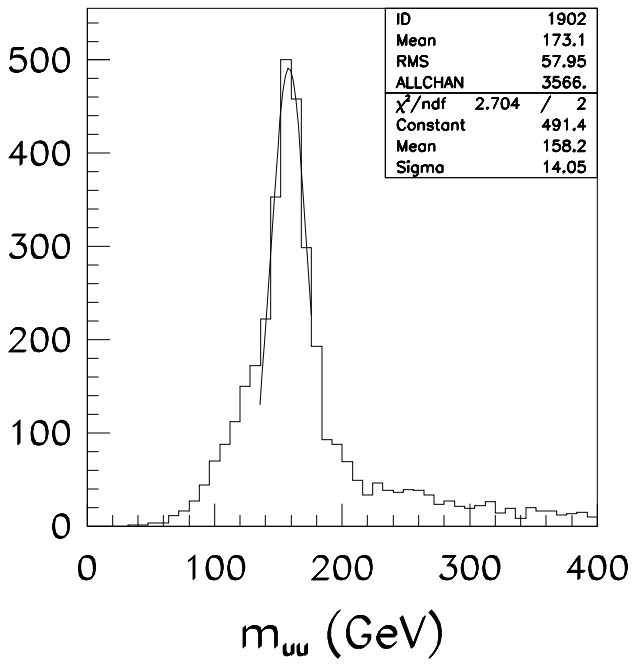
ID 1902
Mean 173.1
RMS 57.95
ALLCHAN 3566.
χ²/ndf 2.704 / 2
Constant 491.4
Mean 158.2
Sigma 14.05
0 100 200 300 400
0 100 200 300 400 500
m_uu (GeV)

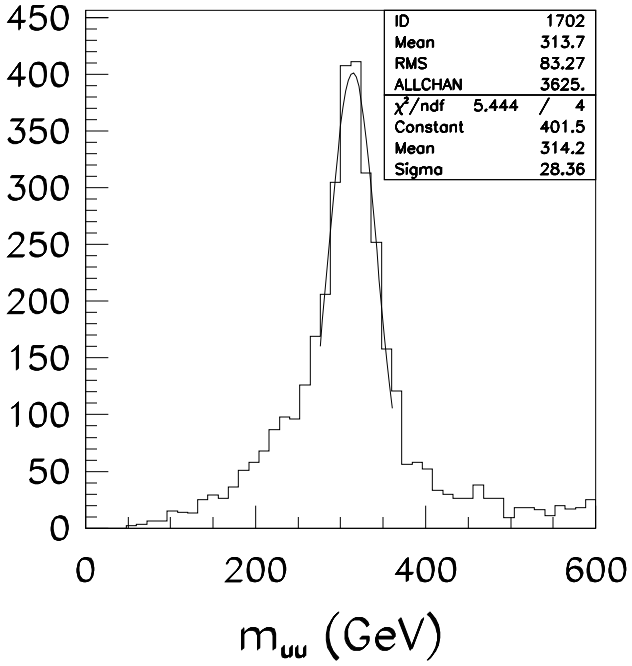
ID 1702
Mean 313.7
RMS 83.27
ALLCHAN 3625.
χ²/ndf 5.444 / 4
Constant 401.5
Mean 314.2
Sigma 28.36
0 200 400 600
0 50 100 150 200 250 300 350 400 450
m_uu (GeV)

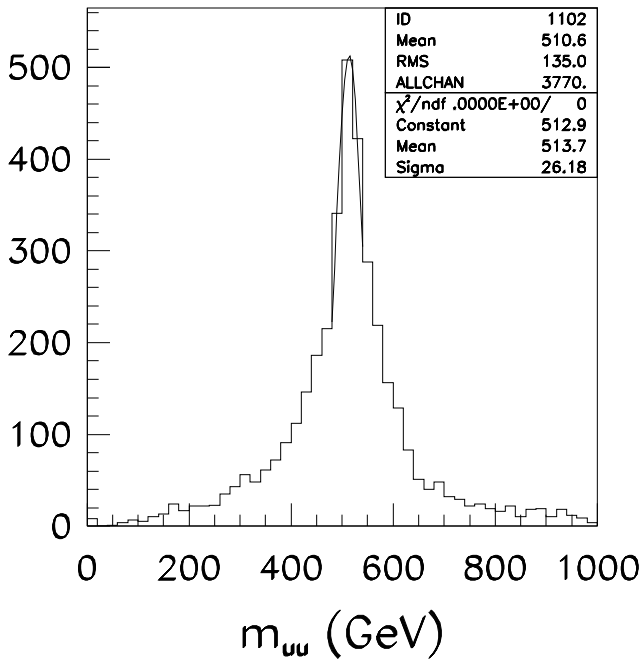
ID 1102
Mean 510.6
RMS 135.0
ALLCHAN 3770.
χ²/ndf .0000E+00 / 0
Constant 512.9
Mean 513.7
Sigma 26.18
0 200 400 600 800 1000
0 100 200 300 400 500
m_uu (GeV)

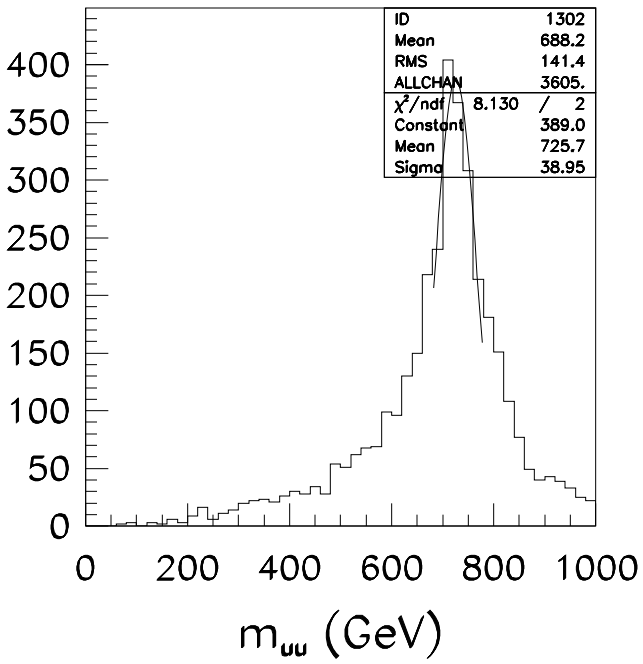
ID 1302
Mean 688.2
RMS 141.4
ALLCHAN 3605.
χ²/ndf 8.130 / 2
Constant 389.0
Mean 725.7
Sigma 38.95
0 200 400 600 800 1000
0 50 100 150 200 250 300 350 400
m_uu (GeV)

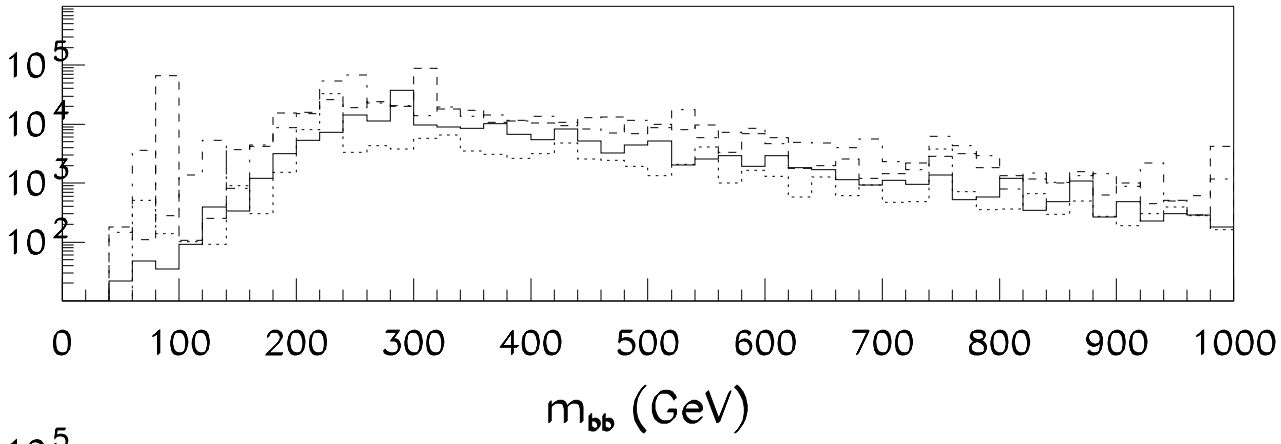
10^5
10^4
10^3
10^2
0
100
200
300
400
500
600
700
800
900
1000
m_{bb} (GeV)

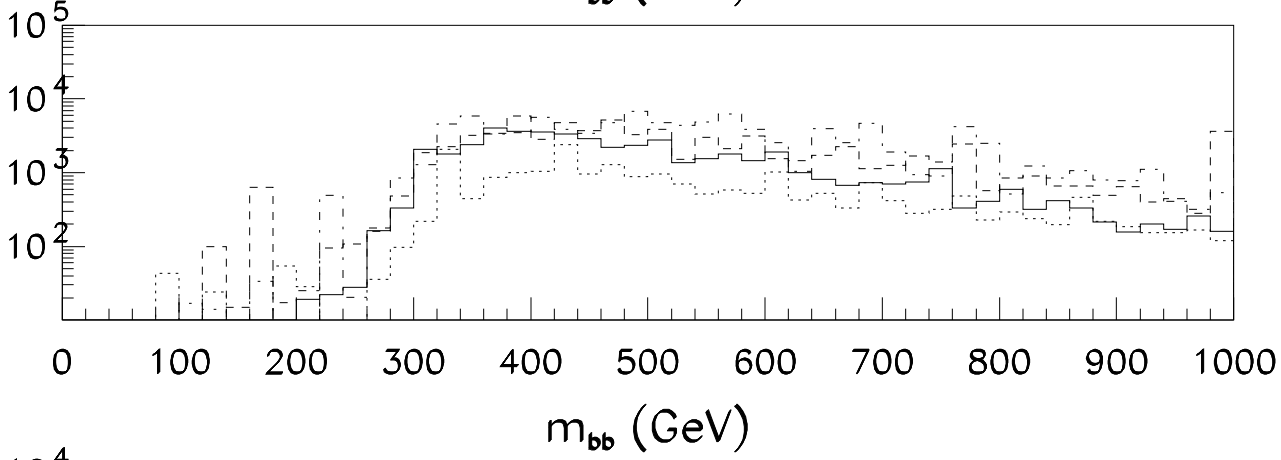
10^5
10^4
10^3
10^2
0
100
200
300
400
500
600
700
800
900
1000
m_{bb} (GeV)

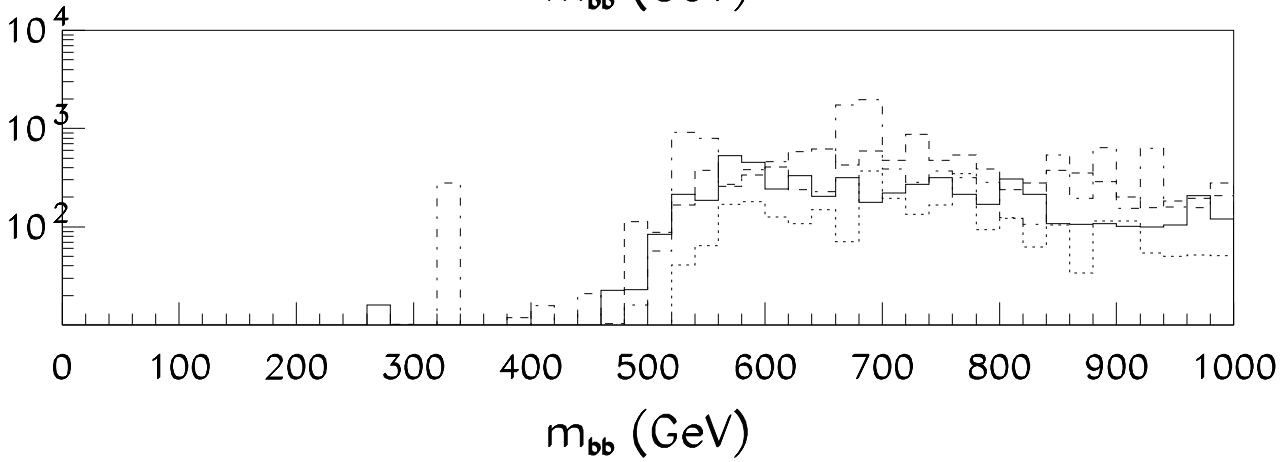
10^4
10^3
10^2
0
100
200
300
400
500
600
700
800
900
1000
m_{bb} (GeV)

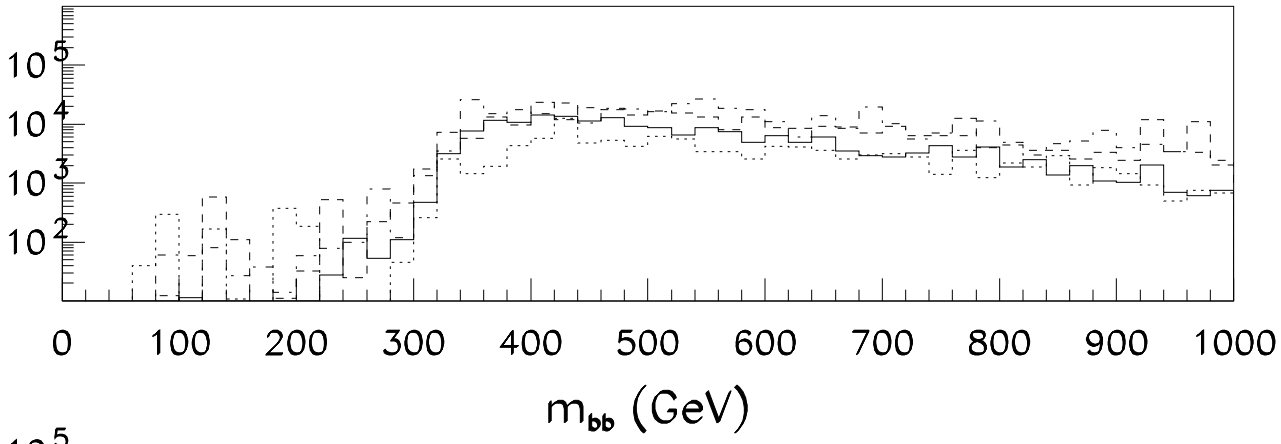
10^5
10^4
10^3
10^2
0
100
200
300
400
500
600
700
800
900
1000
m_{bb} (GeV)

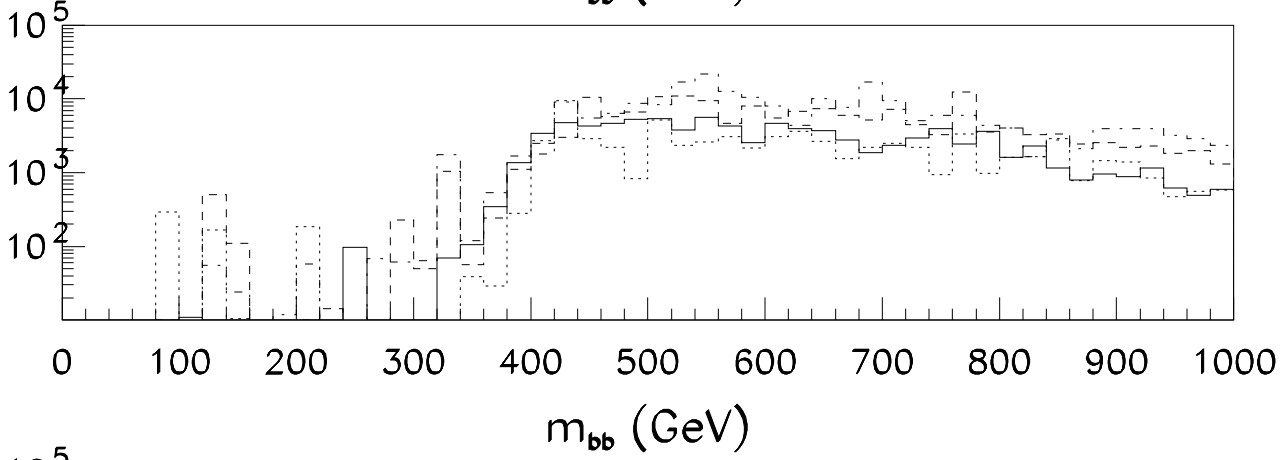
10^5
10^4
10^3
10^2
0
100
200
300
400
500
600
700
800
900
1000
m_{bb} (GeV)

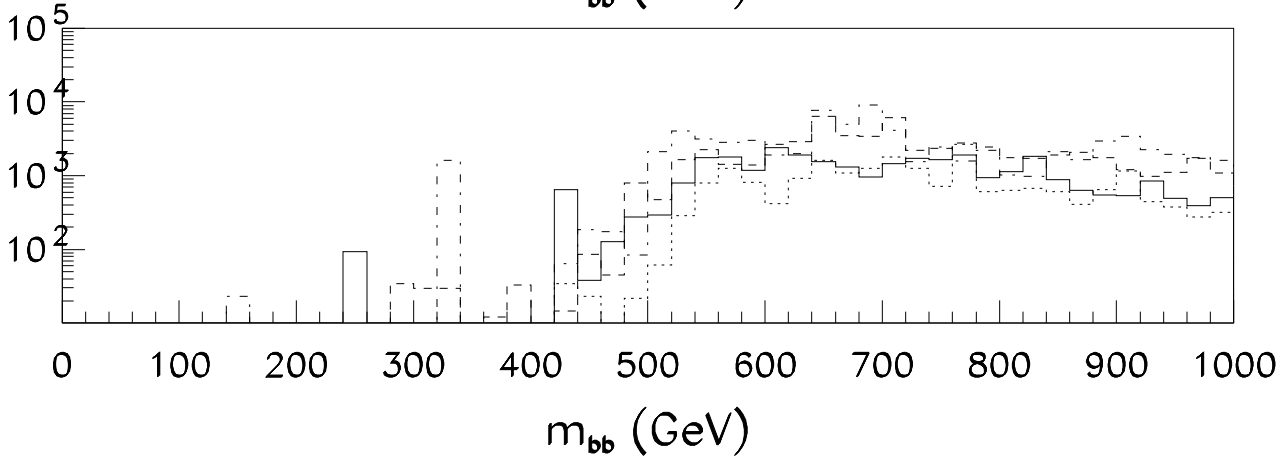
10^5
10^4
10^3
10^2
0
100
200
300
400
500
600
700
800
900
1000
m_{bb} (GeV)

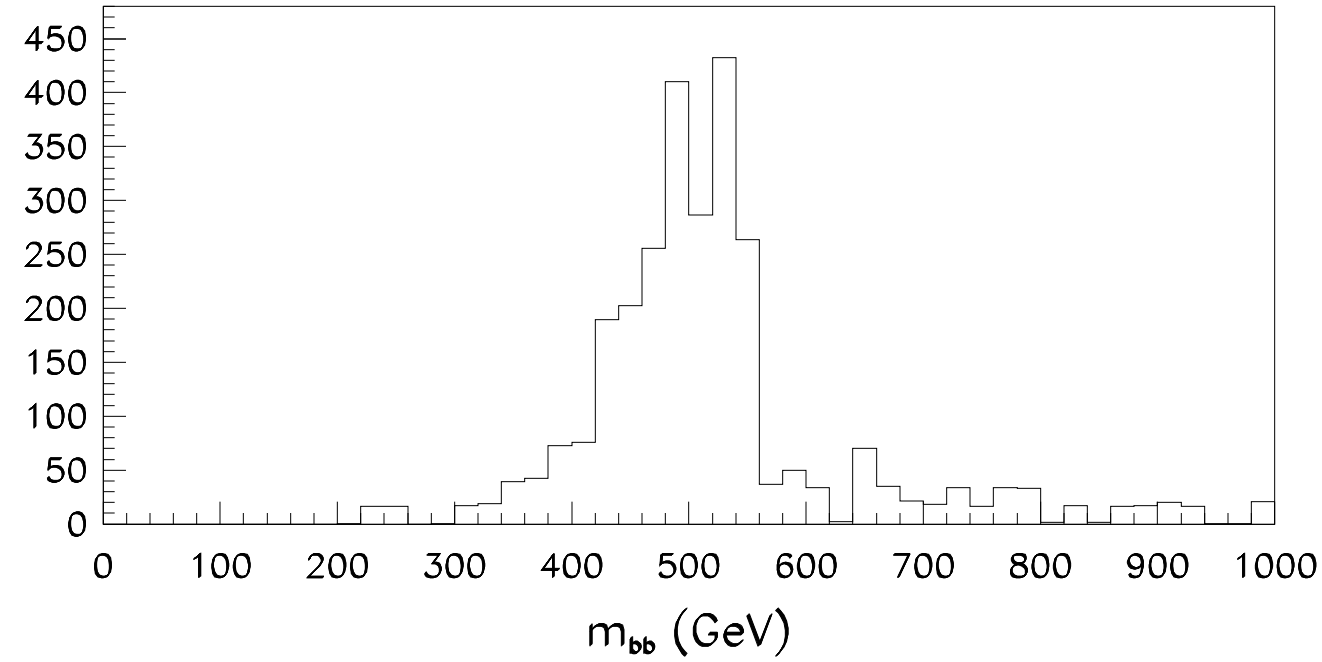
450
400
350
300
250
200
150
100
50
0
0
100
200
300
400
500
600
700
800
900
1000
m_{bb} (GeV)

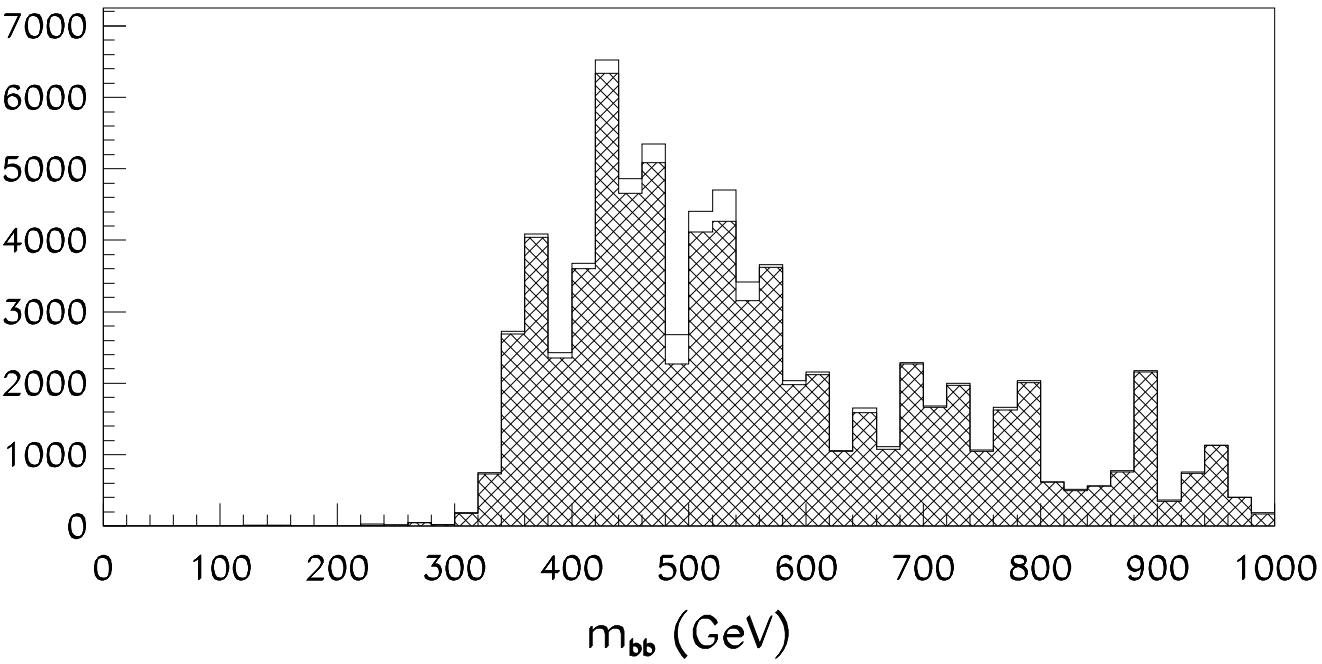
7000
6000
5000
4000
3000
2000
1000
0
0
100
200
300
400
500
600
700
800
900
1000
m_{bb} (GeV)

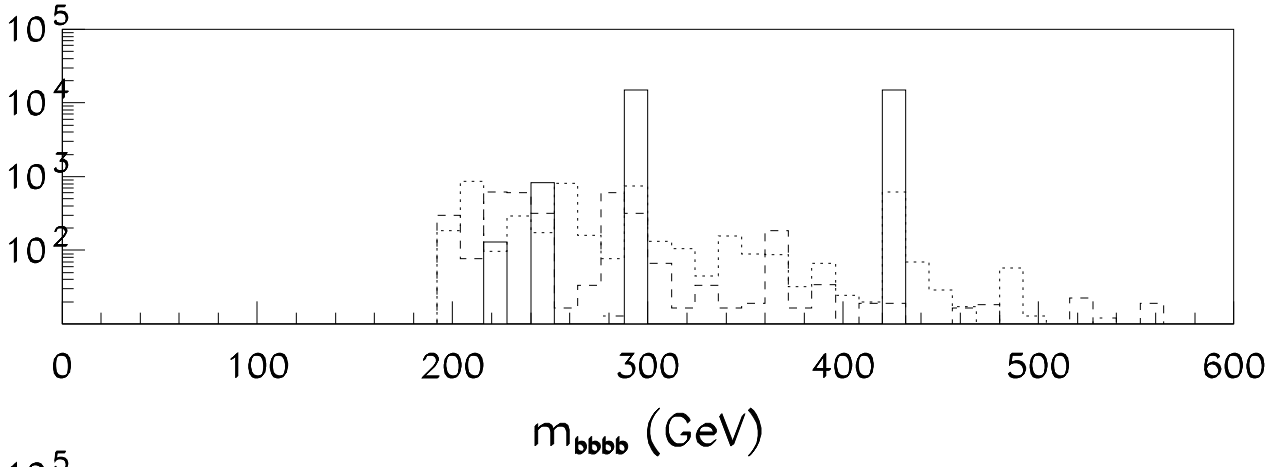
10^5
10^4
10^3
10^2
0
100
200
300
400
500
600
m_{bbbb} (GeV)

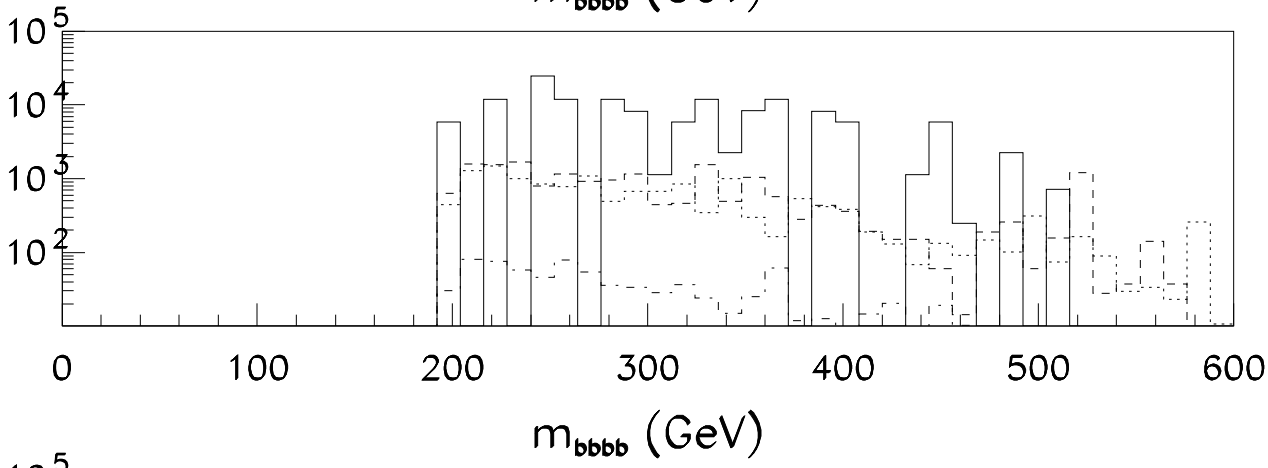
10^5
10^4
10^3
10^2
0
100
200
300
400
500
600
m_{bbbb} (GeV)

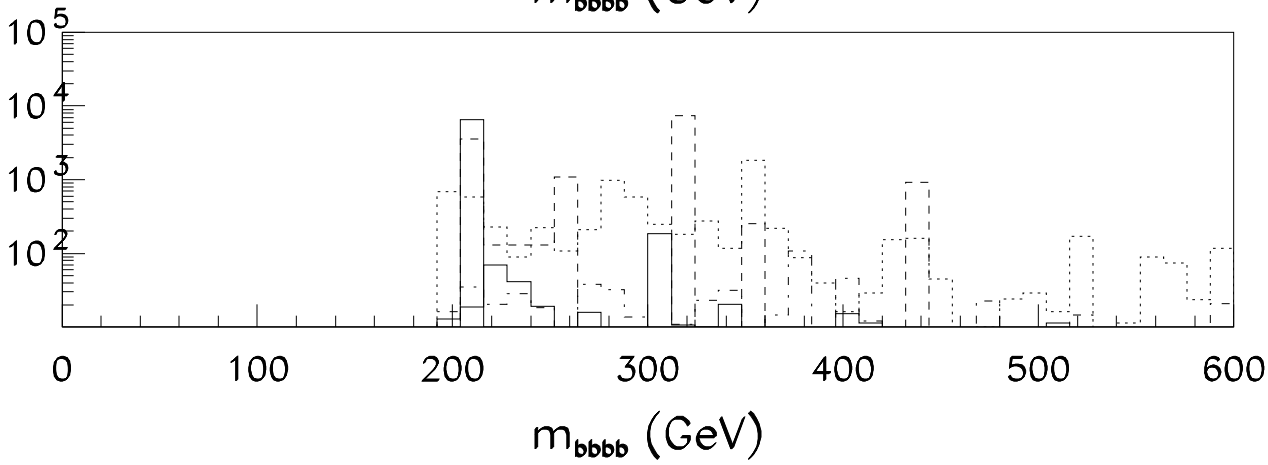
10^5
10^4
10^3
10^2
0
100
200
300
400
500
600
m_{bbbb} (GeV)

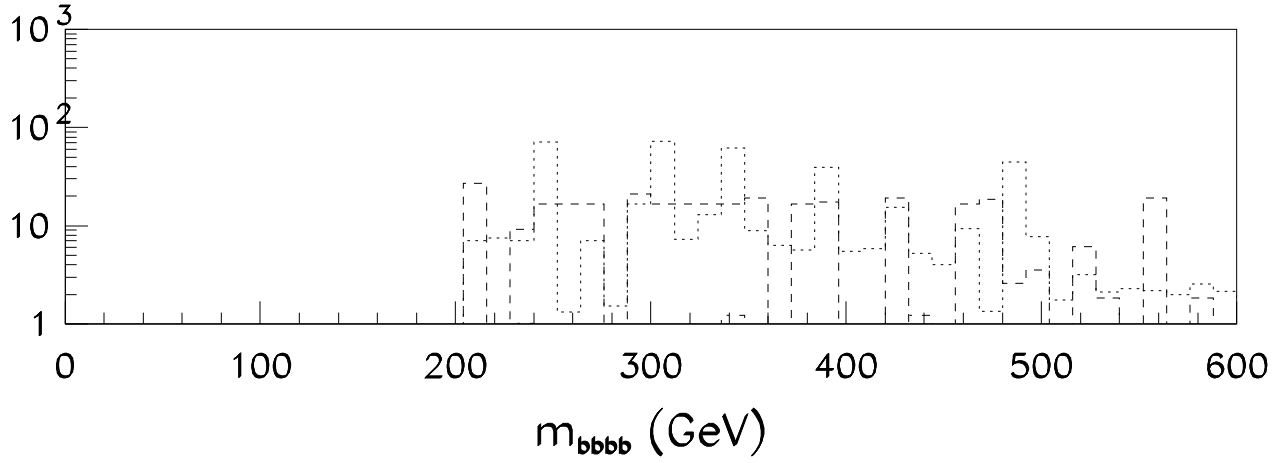
10 3
10 2
10
1
0
100
200
300
400
500
600
m bbbb (GeV)

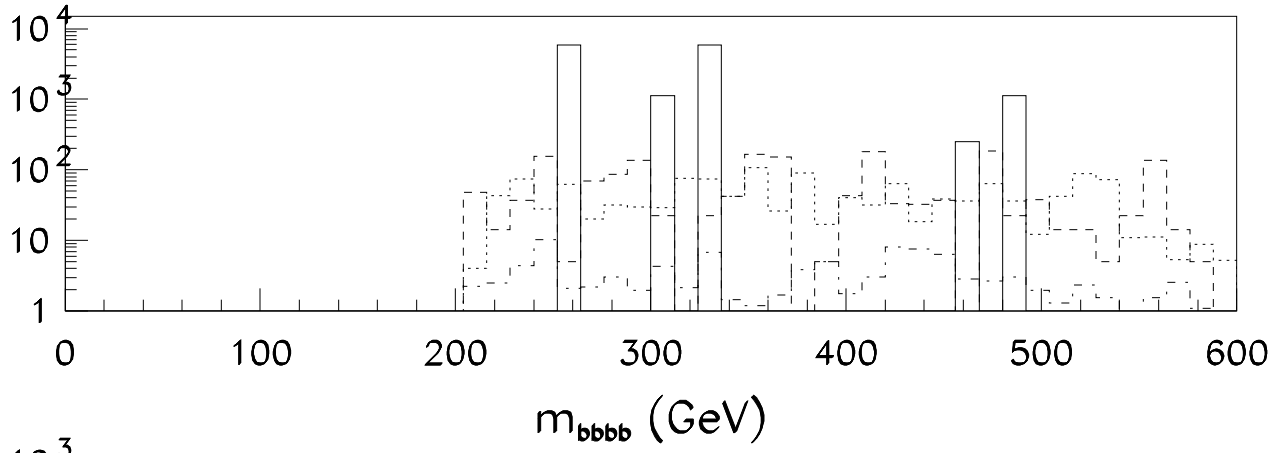
10 4
10 3
10 2
10
1
0
100
200
300
400
500
600
m bbbb (GeV)

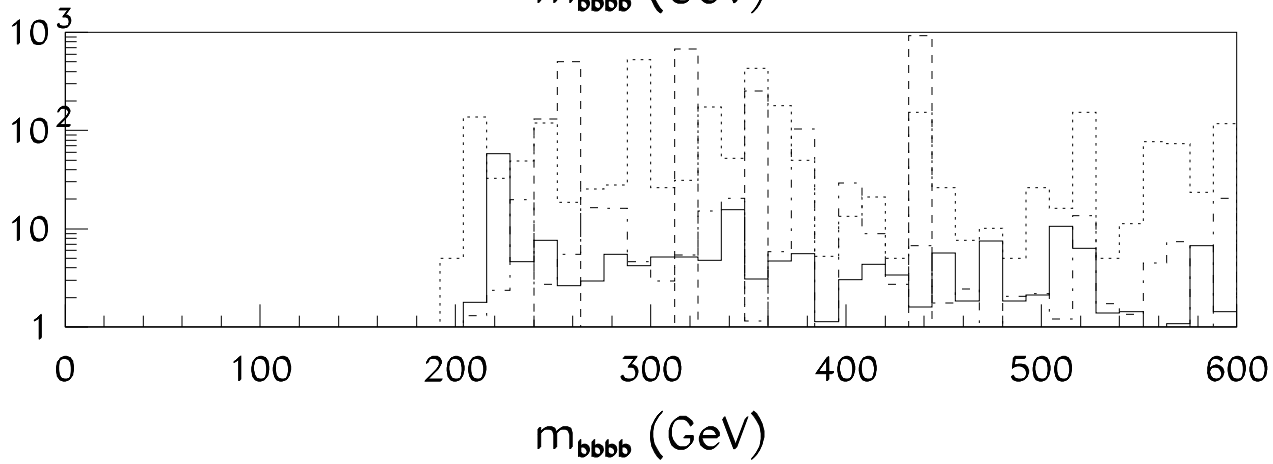
10 3
10 2
10
1
0
100
200
300
400
500
600
m bbbb (GeV)

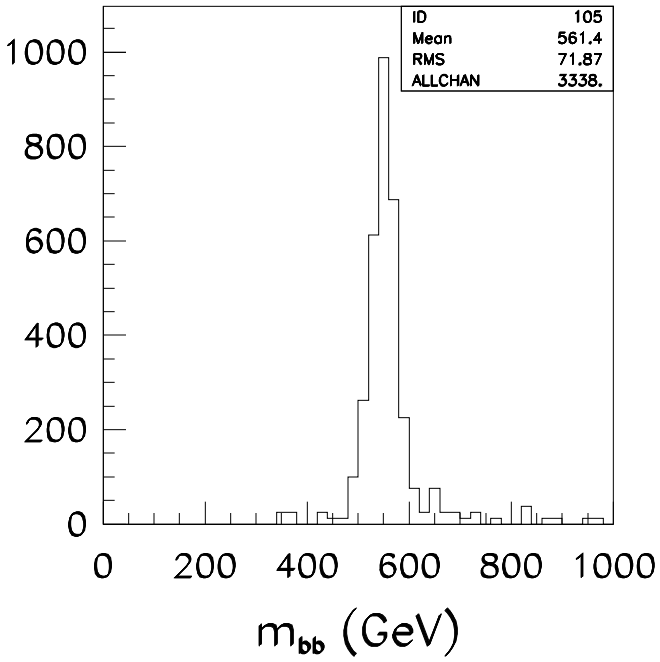
ID 105
Mean 561.4
RMS 71.87
ALLCHAN 3338.
0 200 400 600 800 1000
m_{bb} (GeV)

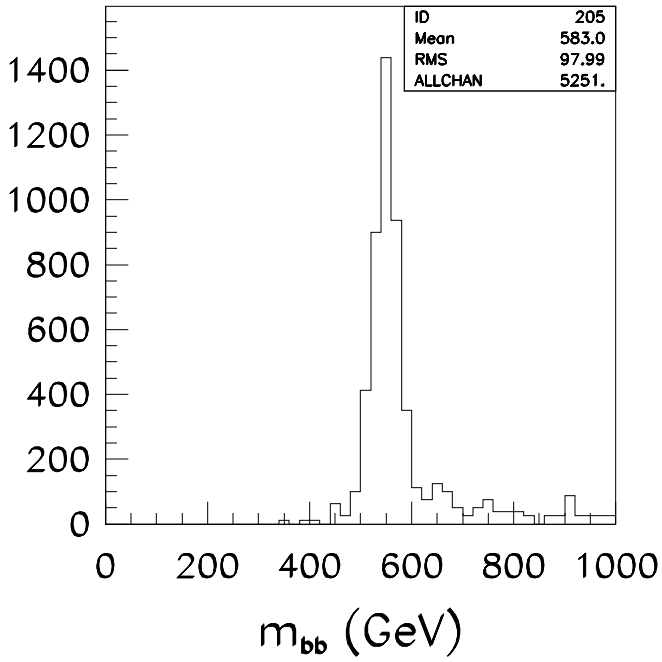
ID 205
Mean 583.0
RMS 97.99
ALLCHAN 5251.
0 200 400 600 800 1000
m_{bb} (GeV)

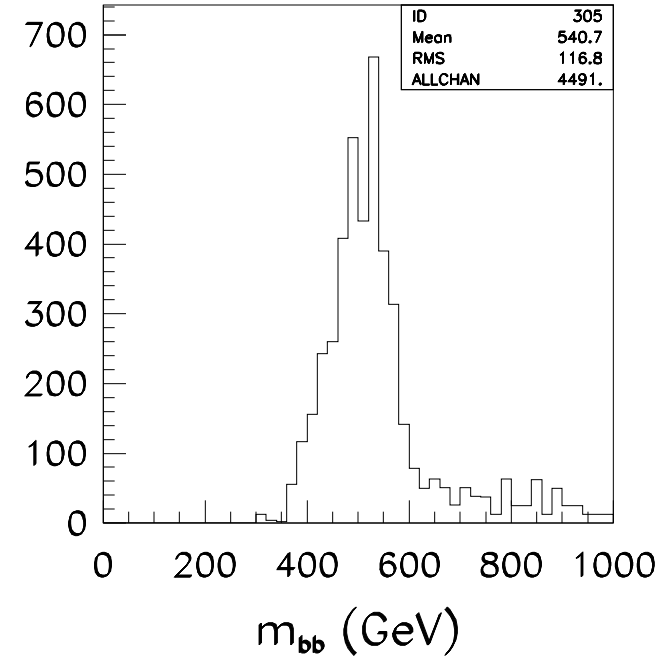
ID 305
Mean 540.7
RMS 116.8
ALLCHAN 4491.
0 200 400 600 800 1000
m_{bb} (GeV)

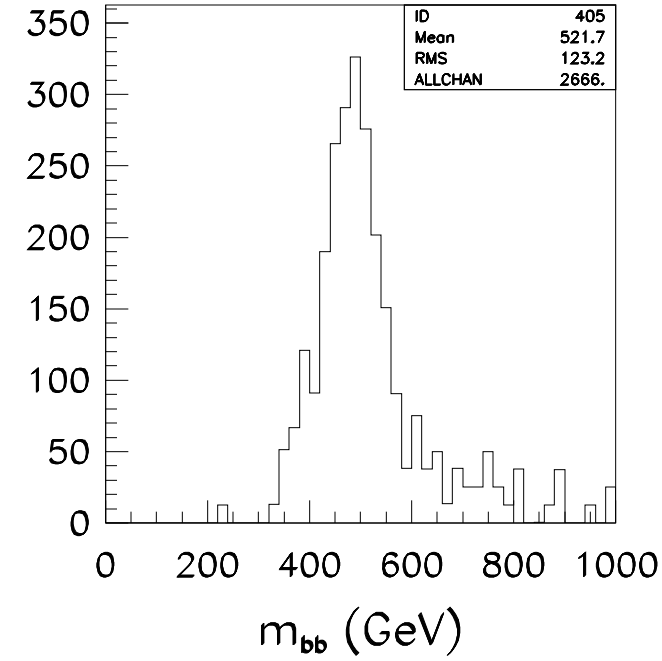
ID 405
Mean 521.7
RMS 123.2
ALLCHAN 2666.
0 200 400 600 800 1000
m_{bb} (GeV)

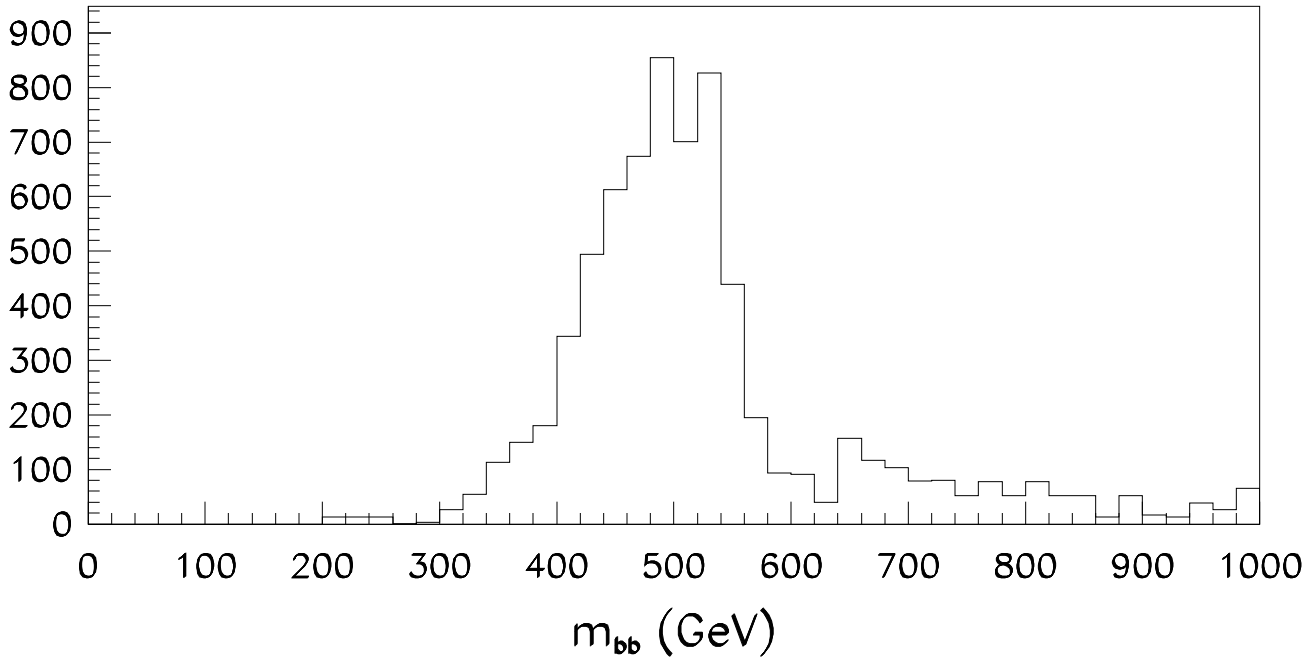
900
800
700
600
500
400
300
200
100
0
0
100
200
300
400
500
600
700
800
900
1000
m_{bb} (GeV)

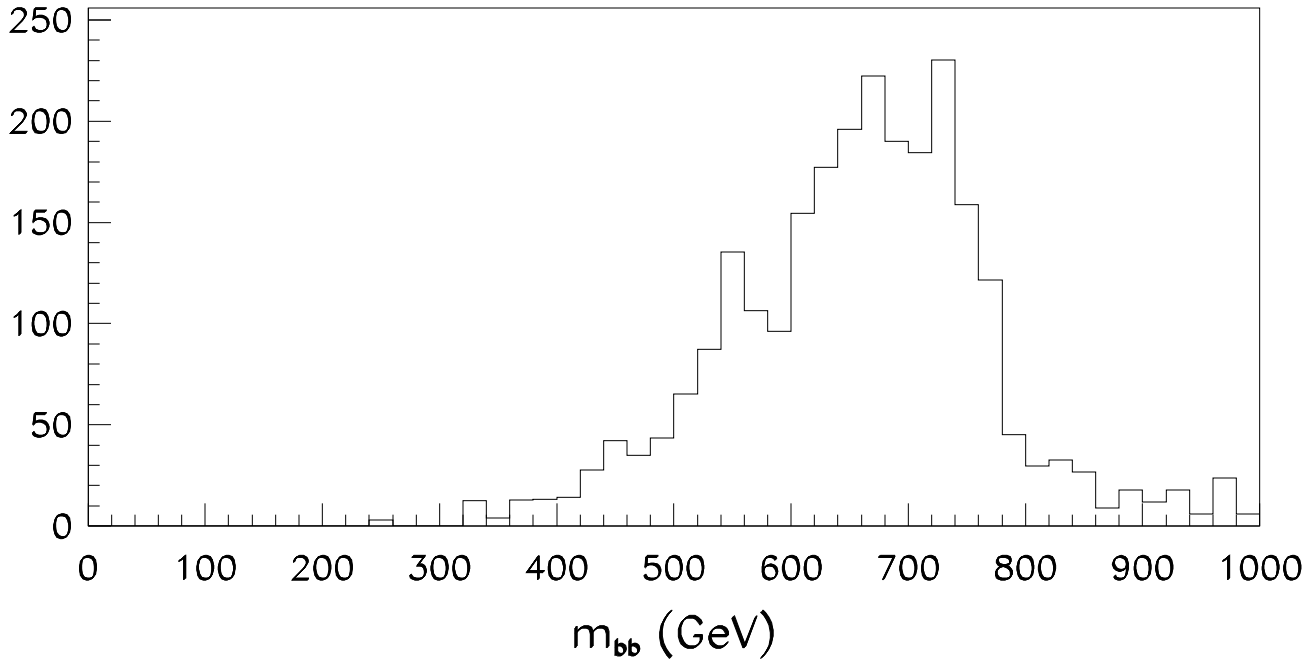
250
200
150
100
50
0
0
100
200
300
400
500
600
700
800
900
1000
m_{bb} (GeV)